

## Ages and Masses of Star Clusters in M33: a Multi-wavelength Study

CAITLIN MOELLER<sup>1,2</sup> AND DANIELA CALZETTI<sup>1</sup>

<sup>1</sup>*University of Massachusetts Amherst  
710 N Pleasant St  
Amherst, MA 01003, USA*

<sup>2</sup>*University of Texas at Austin  
23 San Jacinto Blvd  
Austin, TX 78712, USA*

(Received XXX yyy, ZZZZ; Revised xxx1 yyy1, ZZZ1; Accepted October 19, 2021)

Submitted to AJ

### ABSTRACT

We combine archival images for the nearby galaxy M33 (Triangulum Galaxy) from the ultraviolet (UV) to the infrared (IR) to derive ages, masses, and extinctions for the young star cluster population, and compare our physical parameters with published ones. Our goal is to test the robustness of clusters' ages and masses, and possibly improve on existing ones both by expanding the wavelength range of the spectral energy distribution (SED) fits and by using more recent population synthesis models. The rationale for this experiment is to verify the sensitivity of the clusters' physical parameters to observational setups and model choices that span those commonly found in the literature. We derive the physical parameters of 137 clusters, using SEDs measured in eight UV-to-I bands, including H $\alpha$ , from *GALEX* and ground-based images. We also add the 24  $\mu$ m image from the *Spitzer Space Telescope* to help break some age degeneracies. We find that our derived cluster ages show significant differences with earlier determinations, while the masses remain relatively insensitive to the fitting approach adopted. We also highlight an already known difficulty in recovering old, low-extinction clusters, as SED fitting codes tend to prefer younger, higher extinction solutions when the extinction is a free parameter. We publish updated ages, masses, and extinctions, with uncertainties, for all sample star clusters, together with their photometry; given the proximity of M33, this represents an important population to secure for the study of star formation and cluster evolution in spirals.

*Keywords:* stars: formation — galaxies: star clusters: general —

### 1. INTRODUCTION

Within galaxies, the structures of star formation are a continuous, scale-free hierarchy from parsecs to kiloparsecs (Lada & Lada 2003; Elmegreen 2003; Bressert et al. 2010), which are expected to arise from the self-similar distribution of a turbulence-dominated ISM (Elmegreen & Efremov 1997), mediated by magnetic fields and outflow feedback (e.g., Krumholz et al. 2019b). Star clusters form in the dense regions of the hierarchy (e.g., Elmegreen 2010), and, thus, provide a sensitive probe of the star formation process, while the rest of the hierarchy is quickly dispersed into the stellar field of the galaxy, over timescales of a few tens of Myr (Bastian 2008; Longmore et al. 2014; Grasha et al. 2015, 2017a). Young star clusters contain the majority of the massive stars, which drive the feedback into the surrounding medium and regulate star formation (Krumholz et al. 2019b; Adamo et al. 2020), but most are not bound because they are not dense enough (e.g. Brown & Gnedin 2021). These clusters are dispersed and randomized over short timescales ( $\lesssim 10$  Myr) by a vast array of processes, both internal— such as gas expulsion, stellar evolution, and

two-body relaxation,– and external,– such as tidal shear, random motions, interactions with molecular clouds, and secular evolution of the host galaxy (e.g., Gieles & Bastian 2008).

Deriving accurate ages and masses for star clusters is a key step for linking the small scales of the star formation, i.e., the scales of individual stars, with the large scales of whole galaxies. The physical and chemical properties of star clusters constrain scenarios for their formation and evolution, trace the star formation history of galaxies, constrain models of cloud collapse, provide tests for the origin and persistence of spiral arms, and guide cosmological simulations (Shabani et al. 2018; Li et al. 2018; Adamo et al. 2020; Ballesteros-Paredes et al. 2020). The distribution of cluster masses is a sensitive tracer of formation mechanisms (e.g. Whitmore et al. 1999; Larsen 2002; Gieles et al. 2006b,a; Whitmore et al. 2014; Johnson et al. 2017; Adamo et al. 2020), while the age distribution reveal the cluster disruption mechanisms (e.g., Gieles 2009; Bastian et al. 2012; Silva-Villa et al. 2014; Chandar et al. 2016; Adamo et al. 2017; Messa et al. 2018).

M33 (Triangulum Galaxy) is an excellent laboratory for testing techniques for the derivation of physical parameters of star clusters. This nearby spiral galaxy (850 kpc; Ferrarese et al. 2000) is a member of the Local Group and has a large population of clusters. M33 is close enough that its star clusters can be resolved into stars with the *Hubble Space Telescope*, but distant enough that lower angular resolution facilities can survey it fully. Its modest inclination ( $\sim 52^\circ$ , from NED<sup>1</sup>) minimizes the chance of line-of-sight confusion. At the M33 distance, an angular aperture of  $1''$  radius subtends a  $4.1 \times 5.2 \text{ pc}^2$  spatial region, which is comparable to the size of star clusters (Ryon et al. 2017; Brown & Gnedin 2021). Sarajedini & Mancone (2007) compiled a list of compact sources found in M33, for a total of 451 objects, 255 of which were confirmed to be star clusters. For these clusters, ages and masses were determined in a series of papers by Ma et al. (Ma et al. 2001, 2002a,b,c, 2004a,b), using spectral energy distribution (SED) fitting of medium-band optical filter photometry.

Starting from this compilation, we combine broad-band optical imaging with the two UV *GALEX* images, add the hydrogen recombination line  $H\alpha$ , and include the  $24 \mu\text{m}$  band map from the *Spitzer Space Telescope*, all from archival holdings. Our goal is to leverage the extended wavelength coverage of our photometric measurements to produce accurate ages and masses for the cluster population in this iconic galaxy. The UV is a sensitive discriminator of young versus old populations and, combined with the optical bands, adds a leverage arm for extinction measurements (Calzetti et al. 2015), while  $H\alpha$  tracks the presence of ionizing massive stars. Finally, the  $24 \mu\text{m}$  band traces the emission from the dust heated by the UV photons of young stars ( $\lesssim 100 \text{ Myr}$ , Kennicutt & Evans 2012). Thus the  $24 \mu\text{m}$  emission enables discriminating intermediate age populations ( $\sim 10\text{-}100 \text{ Myr}$ ) when multiple solutions are possible but the  $H\alpha$  emission is no longer present and the UV is mostly yielding degenerate results (Leitherer et al. 1999). The metal abundance of M33 is sufficiently high that we expect significant dust and  $24 \mu\text{m}$  emission in correspondence of its young star clusters. U et al. (2009), Bresolin (2011) and Toribio San Cipriano et al. (2016) report values between  $1/2$  solar and  $\sim 20\%$  above solar<sup>2</sup> for both the young stars and the gas within the inner  $\sim 3.5 \text{ kpc}$  of this galaxy ( $0.4 R_{25}$ ), where most of our sources are located (Figure 1). We compare our results with those of Ma et al. to investigate similarities and differences.

The outline of the paper is as follows. Section 2 describes the cluster compilation of Sarajedini & Mancone (2007). Section 3 discusses the archival imaging data, our processing and photometry. Section 4 describes the models employed for SED fitting and our fitting approach. Section 5 presents the results of the SED fits and our analysis, including comparisons with previous determinations of ages and masses. Section 6 summarizes our findings and conclusions. We present our updated ages and masses and extinctions, as well as photometry, in tabular form for all star clusters in our sample.

## 2. CLUSTER SAMPLE

The clusters in our sample come from a compilation of Sarajedini & Mancone (2007, (henceforth SM2007)) of 451 compact sources in M33, among which the authors identified 255 star clusters using high angular resolution imaging from either the *Hubble Space Telescope* or ground-based facilities. Of these 255 confirmed star clusters, SM2007 lists both ages and masses for a total of 163, as published in a series of papers by Ma et al. (Ma et al. 2001, 2002a,b,c, 2004a,b). Ma et al. derived ages and masses by fitting the population synthesis models of Bruzual & Charlot (1993, with the 1996 improvements) to the SEDs of the sources. The SEDs consisted of photometry in 8 intermediate-band

<sup>1</sup> NED=NASA Extragalactic Database, <http://ned.ipac.caltech.edu/>

<sup>2</sup> We adopt a solar oxygen abundance of 8.69, (Asplund et al. 2009)

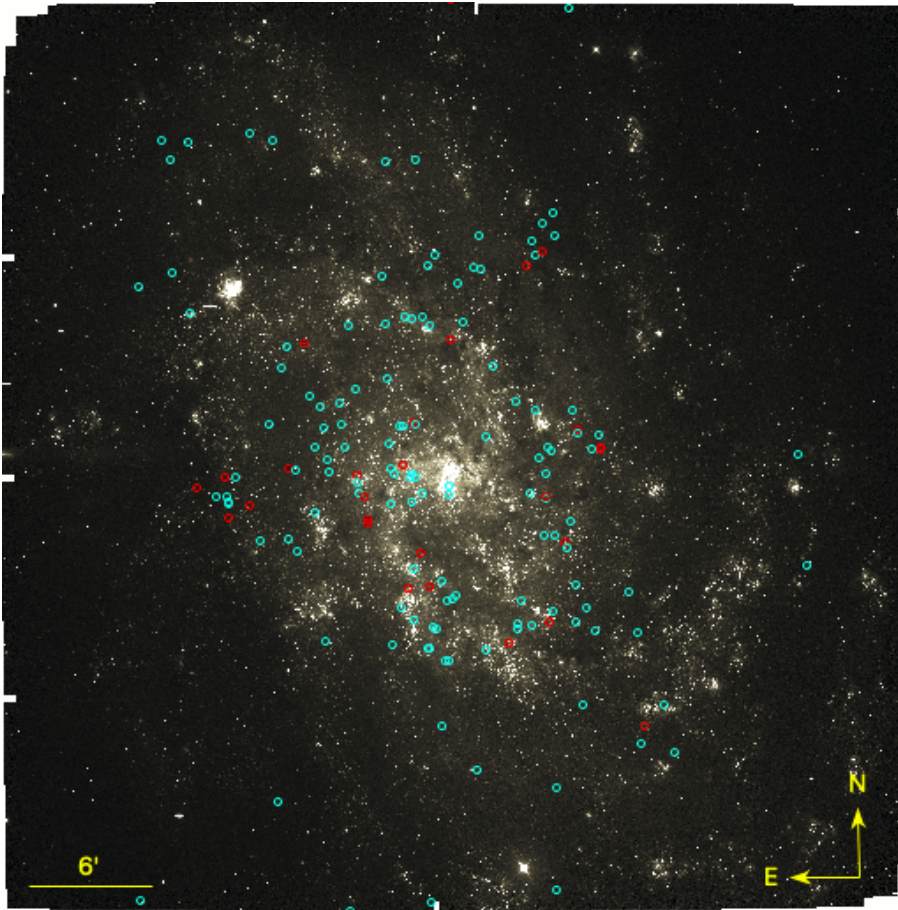


**Figure 1.** Central pointing view of M33 galaxy (U band, from Massey et al. 2006) showing 154 of the 163 star clusters from Sarajedini & Mancone (2007) analyzed in this work. The remaining nine clusters are located in the Northern and Southern pointings, and are not shown here. A scale of 6' correspond to  $\sim 1.5$  kpc at the distance of this galaxy. Cyan circles mark clusters for which SED fits were performed, while red circles mark clusters excluded from the fits, and for which only photometry is provided. See text for more details.

filters in the wavelength range 3800–10,000 Å (Ma et al. 2001). This wavelength range does not enable the authors to constrain uniquely the internal dust reddening of the star clusters, which they either adopt from previous analyses—as in Ma et al. (2001), where the authors use the extinction values of Chandar et al. (1999)—or fix  $E(B-V)$  to a constant value ( $E(B-V)=0.1$ , Ma et al. 2002a). The values of the ages and masses are given without uncertainties. In their SED fits, Ma et al. allowed the metallicity to remain a free parameter, ranging between 3% solar and 1.4 times solar, with the reference solar metallicity being  $Z_{\odot}=0.02$  (Iglesias et al. 1992).

Although optical photometry for the sources is published in SM2007, we do not use these authors' measurements as we aim to derive uniform-aperture photometry for the star clusters, for the purpose of using internally-consistent measures for our SED fitting experiment.

### 3. IMAGING DATA AND PHOTOMETRY

#### 3.1. *The Data*

Ultraviolet, optical and IR images from a combination of space and ground-based imaging data of the M33 galaxy were retrieved from NED, for a total of 10 bands: Far-UV (FUV), Near-UV (NUV), U, B, V, R, I,  $H\alpha$  (6563 Å),  $3.6\mu\text{m}$  and  $24\mu\text{m}$ . The FUV and NUV images trace the youngest stars, with ages  $\lesssim 100$  Myr, while the ionized gas emission at  $H\alpha$  traces even younger stars,  $\lesssim 7\text{--}10$  Myr, although this age limit increases by about a factor of 3 in the presence of binary stars (Xiao et al. 2018). The IR image at  $24\mu\text{m}$  traces the emission of the dust heated by the young stars (Draine & Li 2007; Calzetti et al. 2007).

The *GALEX* satellite (Martin et al. 2005) observed M33 in both the FUV ( $\sim 1530 \text{ \AA}$ ) and NUV ( $\sim 2310 \text{ \AA}$ ) channels with a single pointing of its  $\sim 1.6^\circ \times 1.6^\circ$  field-of-view (FoV) with angular resolution  $\sim 4''\text{--}5''$  (e.g., Dale et al. 2009). The optical band images were obtained by Massey et al. (2006, for U, B, V, R, and I) and Massey et al. (2007, for H $\alpha$ ) at the Mayall 4-m telescope at KPNO, with the Mosaic Camera, with a  $38' \times 38'$  FoV and angular resolution between  $0''.8$  and  $1''$ . To observe the entirety of M33, images were taken in three different pointings: Northern, Central, and Southern. Mosaics at the wavelengths  $3.6 \mu\text{m}$  and  $24 \mu\text{m}$  were obtained with the *Spitzer Space Telescope* IRAC and MIPS cameras, respectively, with angular resolution of  $1''.7$  at  $3.6 \mu\text{m}$  and  $6''.5$  at  $24 \mu\text{m}$  (Fazio et al. 2004; Rieke et al. 2004).

All images were aligned and resampled to the pixel scale of the optical ones ( $0''.27$  per pixel), to preserve the highest possible angular resolution. This facilitates the identification of the location of the SM2007 sources onto the images, and the assessment of whether neighboring sources are present which may affect the ages and mass determinations. The latter step is made necessary by the significantly lower resolution of the *GALEX* and *Spitzer*/MIPS images relative to the ground-based ones.

### 3.2. Photometry

Multi-wavelength photometry was performed on the images using the positions published in the SM2007 catalog. An aperture of  $3''$  in radius was adopted as a compromise between enclosing as much as possible of the UV and IR point spread functions (PSFs) while at the same time minimizing the overlap between photometric apertures of neighboring star clusters. An outer annulus of  $1''.1$  width around each aperture was used to estimate the background and remove it from the aperture measurement. A consequence of the small aperture size is to exclude the wings of the UV and IR PSFs, which leads to an underestimate of the flux of the sources in these bands. We correct for this effect by applying aperture corrections derived by studying the growth curves of isolated sources in the images, and listed in Table 1. The optical broad-band photometry does not require aperture corrections.

We do not apply aperture corrections to the narrow-band photometry, although it is evident from visual inspection that the ionized gas emission is sometimes more extended than the size of our photometric aperture. This aperture subtends a physical radius of 12 pc at the distance of M33, which corresponds to the Strömrgren radius of a  $10^4 M_\odot$ , 5 Myr old star cluster, for an assumed electron density  $n_e \sim 20 \text{ cm}^{-3}$ . In general, our clusters are either less massive or older, but some overflow the aperture with their ionized gas emission. In order to offset this limitation, after running the SED fits, we visually inspect the continuum-subtracted H $\alpha$  image in correspondence of each cluster to ensure that the age results are not driven by an underestimated H $\alpha$  flux.

Filter	Correction Factor
FUV	2.30
NUV	2.36
$3.6\mu\text{m}$	1.22
$24\mu\text{m}$	5.00

**Table 1.** Aperture correction factors applied to the photometry at the indicated wavelengths.

The units of the UV and optical images are count-rates and counts, respectively. We convert those units to physical units of flux density ( $\text{erg s}^{-1} \text{ cm}^{-2} \text{ \AA}^{-1}$ ) using: the stellar photometry of Massey et al. (2006) with the zeropoints published in Zombeck (1990, p. 100) in the case of the *UBVRI* images, the stellar photometry of Massey et al. (2007) with the zeropoints published in the KPNO Mosaic instrument manual<sup>3</sup> in the case of the narrowband H $\alpha$  image, and the conversion factors published in the *GALEX* instrument manual<sup>4</sup> in the case of the UV images. The list of flux conversion factors is in Table 2. Measured photometry for all confirmed 163 star clusters is listed in Table 6. Fluxes are given *prior* to correction for foreground Milky Way extinction, which amounts to  $E(B-V)=0.036$  (Schlafly & Finkbeiner 2011).

To directly observe the presence of line emission in our images, we subtract the stellar continuum as traced by the R-band image from the narrow-band filter targeting the H $\alpha$  line. We rescale the R image prior to subtraction, with

<sup>3</sup> [https://www.noao.edu/kpno/mosaic/manual/mosa3\\_1.html](https://www.noao.edu/kpno/mosaic/manual/mosa3_1.html)

<sup>4</sup> [https://asd.gsfc.nasa.gov/archive/galex/Documents/instrument\\_summary.html](https://asd.gsfc.nasa.gov/archive/galex/Documents/instrument_summary.html)

the scaling factor derived by computing a ratio of the counts in R to the counts in the narrow-band for emission-line-free stellar sources. The narrow-band filter has a FWHM=80.62 Å (Massey et al. 2007) and includes the two [NII](6548,6584 Å) metal lines. We use the ratio [NII]/H $\alpha$ =0.27 published in Kennicutt et al. (2008) to remove the [NII] contamination from the narrow-band filter and obtain an H $\alpha$  image. The stellar continuum subtracted H $\alpha$  images are used solely for visual comparison to confirm the ages of the younger star clusters (<10 Myr) through the presence or absence of excess H $\alpha$  emission. The original, un-subtracted H $\alpha$  images are used for photometry and SED fitting.

The archival *Spitzer* images are already calibrated in surface brightness units of MJy/sr. We convert those to fluxes (erg s<sup>-1</sup> cm<sup>-2</sup>) within our apertures using standard conversion factors, with the appropriate pixel scale of 0".27 per pixel. The 3.6  $\mu$ m photometry is further multiplied by the factor 0.91 to include photometric corrections<sup>5</sup>. The IRAC 3.6  $\mu$ m image is only used to remove the underlying stellar emission from the 24  $\mu$ m image, via the formula:  $F_{24,dust}[\text{Jy}] = F_{24}[\text{Jy}] - 0.035 F_{3.6}[\text{Jy}]$  (Helou et al. 2004; Calzetti et al. 2007). The photometry in these two bands is reported in Table 6 in units of flux. We use the 24  $\mu$ m image mainly to break age degeneracies in the SED fits when the cluster is sufficiently old that the ionized gas emission is no longer present, but still young enough to have UV emission heating the dust.

Visual inspection of all the measured star cluster reveals that 26 out of 163 cannot be retained within our sample for SED fitting for a variety of reasons, as detailed in Table 7. The most common reason is the presence of multiple sources with different colors (likely different ages) within the 3" radius aperture used for the photometry. We thus limit the SED fits to the remaining 137 sources for which we are reasonably confident that one single source is contained within the photometric aperture, or, in case of multiple sources, these show similar colors (likely similar/equal ages).

Filter	Flux Conversion Factor
FUV	1.4E-15
NUV	2.06E-16
U	2.87E-21
B	7.75E-21
V	4.92E-21
R	2.39E-21
I	6.67E-22
H $\alpha$	7.13E-21

**Table 2.** Flux conversion factor used in each filter at UV and optical wavelengths, from either count-rate or counts to erg s<sup>-1</sup> cm<sup>-2</sup> Å<sup>-1</sup>. See text for details.

### 3.3. Measurement Uncertainties

The images at U, B, V, H $\alpha$ , R, and I are sufficiently deep that flux calibration uncertainties dominate the error budget. These are taken from Massey et al. (2006) for the broad-band filters and from Massey et al. (2007) for the H $\alpha$  filter. The uncertainties are listed in Table 3 as uncertainties on the logarithm of the flux. For the optical filters, the value quoted is the largest uncertainty of the sample in each filter.

Uncertainties in the FUV, NUV, and in the (stellar continuum-subtracted) 24  $\mu$ m photometry are dominated by uncertainties in the aperture placement, because of the large PSF size. We calculate these uncertainties by ‘wiggling’ the position of the aperture by one pixel (0".27) in each direction and remeasuring the flux within the aperture. The scatter that results is used in the final error budget, listed in Table 3.

## 4. MODELS AND FITTING APPROACH

### 4.1. Models

The stellar population synthesis models used by Ma et al. (2001) and subsequent papers, i.e., the models of Bruzual & Charlot (1993) with the 1996 updates, are no longer available and did not include nebular emission. More modern

<sup>5</sup> <https://irsa.ipac.caltech.edu/data/SPITZER/docs/irac/iracinstrumenthandbook/46/>

Filter	$\sigma(\log\text{Flux})$
U	0.011
B	0.012
V	0.018
R	0.019
I	0.008
H $\alpha$	0.04
FUV	0.22
NUV	0.15
3.6 $\mu\text{m}$	...
24 $\mu\text{m}$	0.13

**Table 3.** For the optical filters, we quote the calibration error from Massey et al. (2006) and Massey et al. (2007); the value shown is the largest uncertainty for clusters in the luminosity range of our sample; most star clusters have smaller uncertainty in the optical. UV and 24 $\mu\text{m}$  flux errors are calculated through variations of the location of the photometric aperture’s center, which dominate the uncertainty budget.

versions exist, such as those of Bruzual & Charlot (2003) and more recent ones, which also include several updates to the stellar populations characteristics (e.g. Gutkin et al. 2016). Wofford et al. (2016) compared the most recent versions of these models with those generated by Starburst99 (Leitherer et al. 1999; Vázquez & Leitherer 2005) with the addition of nebular lines from YGGDRASIL (Zackrisson et al. 2011), and the BPASS ones (Stanway et al. 2020), finding that all models yield similar result, with low dispersion in the median values of age, mass, and extinction.

In this analysis, we adopt the Starburst99+YGGDRASIL simple stellar population (SSP) models, with the assumption that star clusters can be reasonably approximated by an instantaneous burst (single) population (Wofford et al. 2016). The models are deterministic, meaning that the stellar Initial Mass Function (IMF) is assumed to be fully sampled from the lowest to the highest stellar masses. This is not the case for star clusters with masses  $< 3,000\text{--}5,000 M_{\odot}$  (e.g., Cerviño et al. 2002), implying that the age and mass determinations for clusters below this mass limit will carry an uncertainty larger than the formal one we quote. While the correct approach for such low mass clusters is to use a Bayesian fitting method that returns full posterior probability distributions for a stochastically sampled IMF (e.g., SLUG Krumholz et al. 2019a), this approach is beyond the scope of our current work.

Starburst99 (Leitherer et al. 1999) spectral synthesis models were generated with a Kroupa (2001) IMF in the range 0.1–120  $M_{\odot}$  and metallicity  $Z = 0.02$ . This metallicity value is higher than the mean value of the M33 region where most of our clusters are located,  $\sim 0.5\text{--}1$  solar, but we choose it for the following three reasons: (1) the model ‘ingredients’ are inconsistently sampled for metallicity below solar (Vázquez & Leitherer 2005); (2) the next model metallicity available is about 1/2 solar, at the lower end of the range for our clusters; and (3) ages and masses derived via multi-band SED fits are relatively insensitive to variations of a  $\sim 2.5$  factor in metallicity of the models, as shown in Figures 13 and 14 (see, also, de Grijs et al. 2005, and SM2007). We do expect star clusters older than a few 100 Myr to have lower metallicity than younger ones, as also found by Ma et al. (2001). However, our study is mostly interested in star clusters younger than  $\approx 1\text{--}3 \times 10^8$  yrs, which is the age range where we expect the addition of UV, H $\alpha$ , and dust emission (24  $\mu\text{m}$ ) tracers to have the most impact on the clusters’ physical parameters determination.

The models utilize the Padova tracks with AGB treatment, to better represent intermediate and old stellar populations (Girardi et al. 2000; Vázquez & Leitherer 2005) and are generated for the age range 1 Myr–13 Gyr; the age steps are 1 Myr in the 1–15 Myr range, 10 Myr in the 20–100 Myr range, 100 Myr in the 200–1000 Myr range, and 1 Gyr in the 2–13 Gyr range. The addition of nebular emission lines via YGGDRASIL (Zackrisson et al. 2011) includes a covering factor of 50% for the gas emission, to account for leakage of ionizing photons out of HII regions (e.g., Calzetti et al. 2021). The models assume non-rotating, single stars. There is, however, increasing evidence that stellar population models implementing rotating, binary stars are better fits for data of star clusters, especially at young ages and low metallicities (Stanway et al. 2020). Variations at the young ages can be as large as a factor 2–3 (Wofford et al. 2016). However, given that M33 star clusters span a range of ages much larger than this scatter and that the galaxy is fairly metal rich, we will not include effects of rotating and binary stars, although this should be noted as a point for future investigations. We note that the Starburst99+YGGDRASIL models do not include Very Massive

Stars ( $>150 M_{\odot}$ ) either, which are known to be present in young star clusters (e.g. Crowther et al. 2010; Smith et al. 2016) and are included in more recent populations synthesis models (e.g. BPASS, Eldridge et al. 2017; Stanway & Eldridge 2018). Our goal in choosing the Starburst99+YGGDRASIL models is to remain close to the astrophysical assumptions used in the stellar population synthesis models used by Ma et al. (2001) and subsequent papers.

The effects of dust on the stellar population SEDs are applied via a starburst attenuation curve (Calzetti et al. 2000), with the equation:

$$F(\lambda)_{mod,ext} = F(\lambda)_{model} 10^{[-0.4E(B-V)k(\lambda)]}, \quad (1)$$

where  $k(\lambda)$  is the starburst curve, and  $E(B-V)$  is the color excess applied to the SEDs. We generate models with the color excess range  $E(B-V) = 0-1$ , with step 0.02. As we use the directly measured cluster photometry of Table 6, the small foreground Milky Way extinction with  $E(B-V) = 0.036$  is corrected with the Milky Way curve of Fitzpatrick (1999).

The dust-attenuated SEDs are then convolved with the transmission curve of each of the UV and optical filters to produce synthetic luminosities in 8 bands, that are normalized to the default mass of Starburst99,  $10^6 M_{\odot}$ . The synthetic photometry so obtained is then used to fit the observed SEDs of the star clusters.

#### 4.2. Fitting Approach

Ma et al. (2001) and subsequent works by these authors estimated the ages and masses of the star clusters in M33 by using a least square fit between observed and synthetic photometry (Kong et al. 2000). We adopt the same approach, described by:

$$\chi^2(n, t, E(B-V), M) = \sum_{i=1}^8 [F(\lambda_i, n)_{obs} - F(\lambda_i, t, E(B-V), M)_{mod,ext}]^2 / \sigma(\lambda_i, n)^2 \quad (2)$$

where,  $F(\lambda_i, n)_{obs}$  is the observed flux density of the  $n$ th star cluster in the  $i$ -th band,  $F(\lambda_i, t, E(B-V), M)_{mod,ext}$  is the synthetic flux density of the models described in the previous section in the  $i$ -th band, and  $\sigma(\lambda_i, n)$  is the uncertainty in the observed flux density; the model populations are a function of the age  $t$ , the color excess  $E(B-V)$ , and the cluster mass  $M$ . The index  $i$  runs from 1 to 8, which is the number of bandpasses in our SEDs. The goal is to minimize the reduced  $\chi^2_{red} = \chi^2 / (N_{freed} - 1)$ , where  $N_{freed} = 5$  is the number of degrees of freedom for 8 independent datapoints and 3 parameters. Uncertainties in the fits are obtained by investigating the distribution of  $\chi^2_{red}$  values around the minimum, as described in Calzetti et al. (2021); we also study the  $\chi^2_{red}$  distributions to ensure that our best fits are not the result of local minima.

Ma et al. (2001) explored solutions for three different metallicities –  $Z = 0.0004, 0.004, \text{ and } 0.02$ , finding that older star clusters are better fit by models with lower metallicity. However, as already discussed above, these authors could not constrain the amount of intrinsic extinction in the clusters, due to the limited wavelength range of their SEDs, and either adopted a constant value of  $E(B-V) = 0.1$  or values derived by previous authors. Conversely, we employ a single metallicity value, but extend the wavelength range of the clusters' SEDs to better separate age from extinction. Our goal is to understand how changing the wavelength range of the SEDs and the fitting approach affects the values of ages  $< 1-3 \times 10^8$  yr, where the age-extinction degeneracy is generally pronounced. The inclusion of UV colors provides, theoretically, a better handle of the effects of extinction, and, when accompanied by the  $U-B$  color, provides a sensitive discriminant for separating age from extinction. With the addition of the  $H\alpha$  emission we can better identify clusters younger than  $\sim 7-8$  Myr, a regime where the above colors are often of inconclusive diagnostics (see discussions in Boquien et al. 2009; Calzetti 2013; Calzetti et al. 2015). Furthermore, We use the  $24\mu\text{m}$  emission as a discriminant for multiple-age solutions, i.e., for the presence of multiple minima in the distribution of the  $\chi^2_{red}$  values. For clusters with two viable ages with significant difference (e.g. 8 Myr and 80 Myr), a visual check of the  $24\mu\text{m}$  emission at the location of the cluster is used as the deciding factor. The  $24\mu\text{m}$  dust emission has been shown to follow closely the  $8\mu\text{m}$  emission in HII regions (Relaño & Kennicutt 2009), and the latter has been shown to decrease dramatically with increasing age of the star cluster out to at least 300–400 Myr (Lin et al. 2020). Sharma et al. (2011) showed that most of the  $24\mu\text{m}$  bright sources in M33 are generally younger than 10 Myr.

## 5. ANALYSIS AND RESULTS

### 5.1. Ages, Masses, and Extinctions

The ages, masses, and extinctions of the 137 star clusters in M33 obtained from the photometry in Table 6 via SED fitting are listed in Table 5, together with the ages and masses compiled by SM2007. Examples of SEDs and their best fits are shown in Figures 2, 3, and 4, for five cases each with ages  $\leq 10$  Myr, 10 Myr–100 Myr, and  $>100$  Myr, respectively. As expected, the youngest star clusters usually display  $H\alpha$  in emission and strong UV fluxes relative to the optical ones, the oldest ( $>100$  Myr) clusters have red SEDs with no  $H\alpha$  emission, while the clusters with ages intermediate between these two often display blue SEDs, with significant UV emission, but no or little measurable  $H\alpha$  emission. A few individual cases are shown in Figures 5, 6, and 7 for the young, intermediate, and old stellar population cases; here we display, in addition to the observed SED and its best fit, image cutouts centered on the cluster, in the light of  $H\alpha$  (both continuum-subtracted and non) and  $24\ \mu\text{m}$ , to show the cluster’s appearance at these wavelengths. Young clusters show clear  $H\alpha$  and  $24\ \mu\text{m}$  emission, which decreases in intensity with increasing age. In Figure 8, the case of a star cluster with extended  $H\alpha$  is shown; in this case, the ionized gas emission has developed a ‘ruptured bubble’ morphology and our photometric aperture only captures a fraction of the  $H\alpha$  emission from this cluster, which explains the faintness of the  $H\alpha$  line in the SED plot.

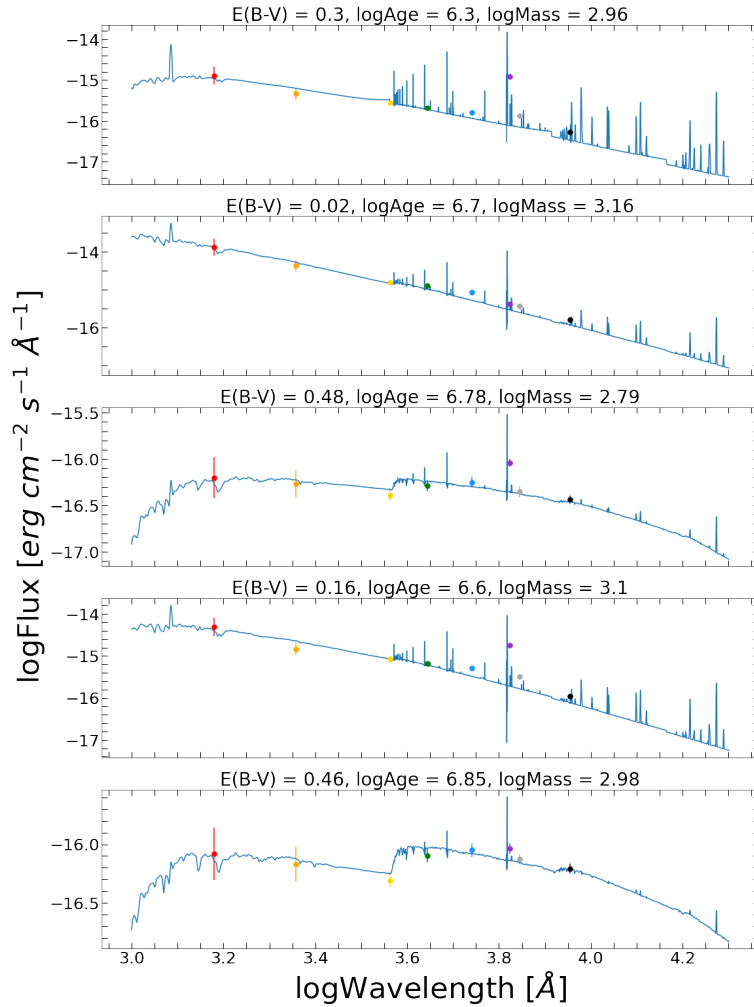


**Figure 2.** Five example SEDs of star clusters with  $< 10$  Myr. Beginning at the top plot, the clusters shown are 42, 70, 77, 79, and 111. The best fit extinction, age, mass of each cluster are listed at the top of each panel, with the age and masses in logarithmic scale. Units are: mag for  $E(B-V)$ , yr for ages and  $M_{\odot}$  for masses.

The distributions of ages, masses, and extinctions are shown in graphical form in the two panels of Figure 9, where the masses and  $E(B-V)$  are plotted as a function of the ages in the left and right panels, respectively. Statistics for the star clusters are also given in Table 4.



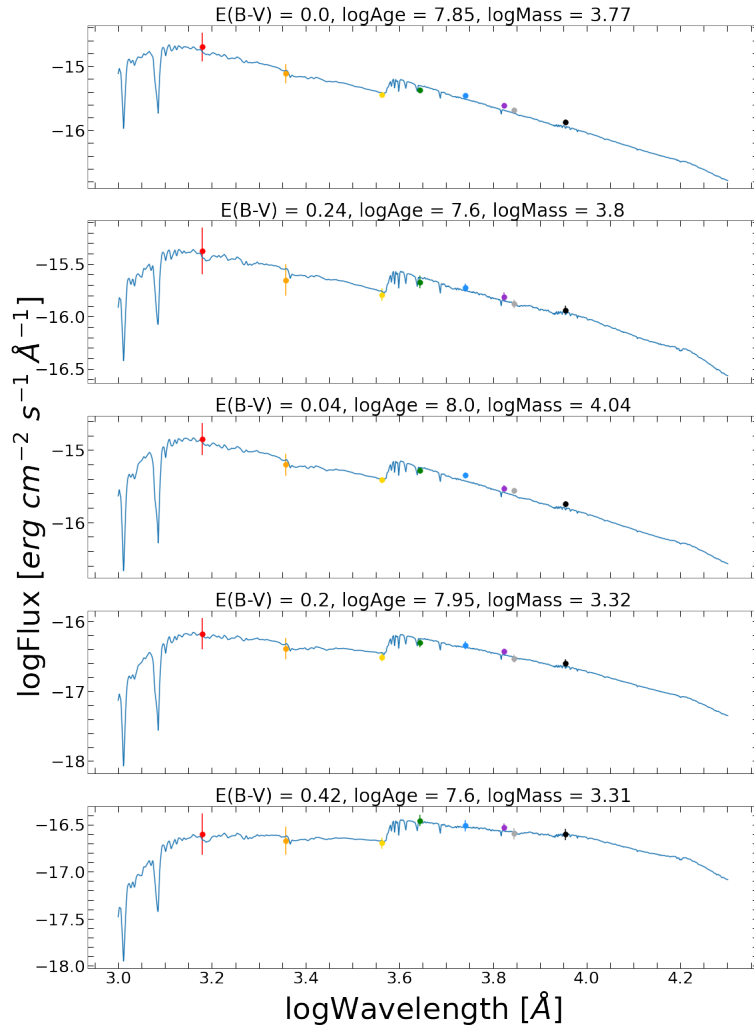


**Figure 3.** Five example SEDs of star clusters in the age range 10–100 Myr. Beginning at the top plot, the clusters shown are 22, 33, 52, 61, and 134. See caption of Figure 2 for more details.

	$\leq 10$ Myr	10–100 Myr	$> 100$ Myr
Total clusters in age bin	21	37	79
Clusters $\geq 3000 M_{\odot}$	2	30	75
Clusters $\geq 5000 M_{\odot}$	1	20	62

**Table 4.** Statistics on the distribution of ages and masses for the star clusters in M33, broken into three age bins and three mass bins. 90% of the clusters with age  $\leq 10$  Myr have masses below  $3,000 M_{\odot}$ , while 95% of clusters older than 100 Myr have masses above this value.

Most (90%) of the clusters younger than 10 Myr have masses below  $3,000 M_{\odot}$  and only one is more massive than  $5,000 M_{\odot}$  (Table 4), indicating that cluster masses in this age range are uncertain due to stochastic sampling of the stellar IMF (Adamo et al. 2017). The general impact of stochastic sampling on our age and mass determinations for these young clusters is that the clusters could be moderately more massive and a factor of a few older than what we find; the discrepancies between deterministic and stochastic models decrease for older ages and higher mass clusters (Krumholz et al. 2015, , their Figure 14). Older age clusters are usually more massive, as seen in the left hand-side panel of Figure 9, where the model line marks the standard lower luminosity limit for the detections. As expected, the masses we determine at a given age are above the model line (SM2007; see, also, Adamo et al. 2017). The trend for older clusters to be more massive than younger ones at the low mass end is simply due to fading with age, while the

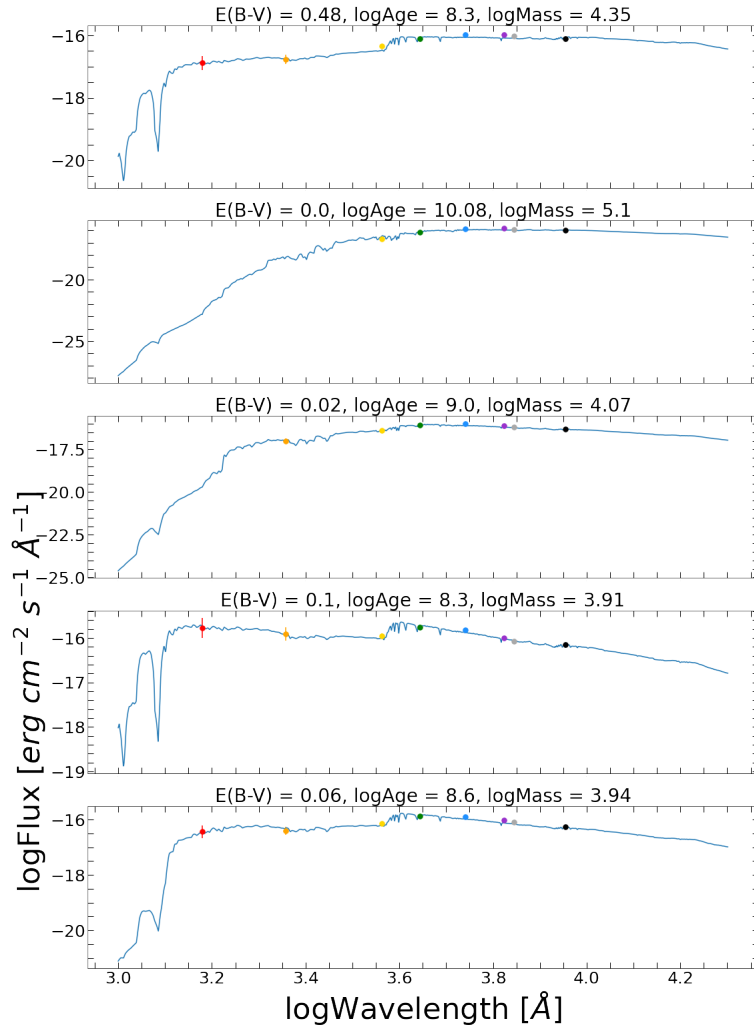


**Figure 4.** Five example SEDs of star clusters with  $> 100$  Myr age. Beginning at the top plot, the clusters shown are 24, 48, 80, 105, and 137. See caption of Figure 2 for more details.

observation that they are more massive also at the high end of the mass distribution is the well known size-of-sample effect (Hunter et al. 2003). Figure 10 compares our derived masses with those reported by SM2007. The masses scatter around the 1-to-1 line (in log scale) up to  $\sim 10^4 M_{\odot}$ , and our masses become systematically smaller than those reported in SM2007 at higher values. We attribute this discrepancy to the systematically younger ages we derive from our SED fits, which yields lower masses at a given luminosity. Overall, however, the masses derived in this work and those reported by SM2007 track each other reasonably well. The most massive clusters in this sample are about  $2 \times 10^5 M_{\odot}$ , which is typical of spiral galaxies (Larsen 2009; Adamo & Bastian 2018).

A comparison of the ages derived here with those reported in SM2007 reveals, conversely, major discrepancies, as shown in Figure 11. There are several instances in which clusters that were classified as ‘old’ (older than  $\sim 100$  Myr) in SM2007 are found to be around or younger than 10 Myr with our SED fits and visual checks of the  $H\alpha$  images. At the opposite end, many clusters that are given ages  $\lesssim 10$  Myr in SM2007 are found to have much older ages by our SED fits,  $> 30$ – $40$  Myr. One important characteristic of our results is that we find less than a handful of clusters with ages  $> 10^9$  yr, while SM2007 list many. Whitmore et al. (2020) discusses in detail that there appear to be a limitation in the ability of SED fitting routines to identify old clusters correctly: in the presence of a ‘red’ SED, fitting routines often prefer a highly-extincted, younger age solution to an extinction-free, older age solution. A work-around to this issue is to impose a limit to the highest value of  $E(B-V)$  that an older star cluster can have, in order to force an older age solution (as discussed in Whitmore et al. 2020). This approach was adopted by Ma et al. (2004b) for a set of the

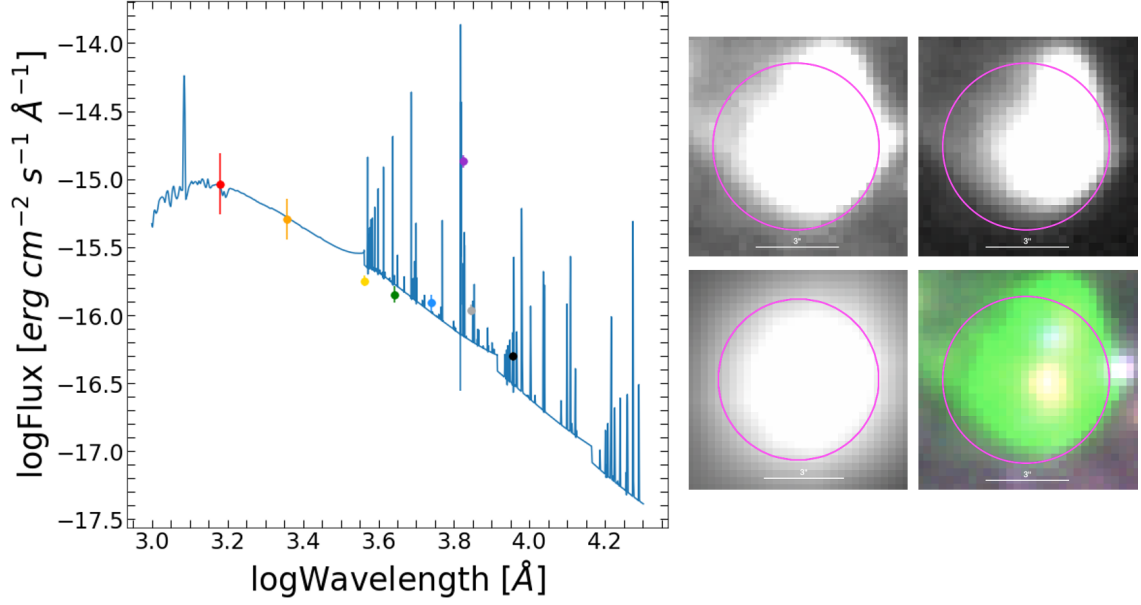


**Figure 5.** Cluster 58 is an examples of a  $<10$  Myr cluster. Its best fits values are: age = 2 Myr, mass =  $890 M_{\odot}$ , and  $E(B-V) = 0.32$  mag. The eight-band photometry with the best fits SED model (as a blue line) are shown in the left panel. The four small panels to the right show for the cluster, beginning at the top left and moving clockwise: the  $H\alpha$  emission, the continuum-subtracted  $H\alpha$  emission, an RGB color composite (red = R band, green =  $H\alpha$  band, and blue = U band), and the stellar-subtracted  $24\mu\text{m}$  emission. The magenta circle shows the size of the aperture used for the photometric measurements. The scale bar below the aperture represents  $3''$ . The flux scale of the images is linear, however the upper and lower limits differ between bands.

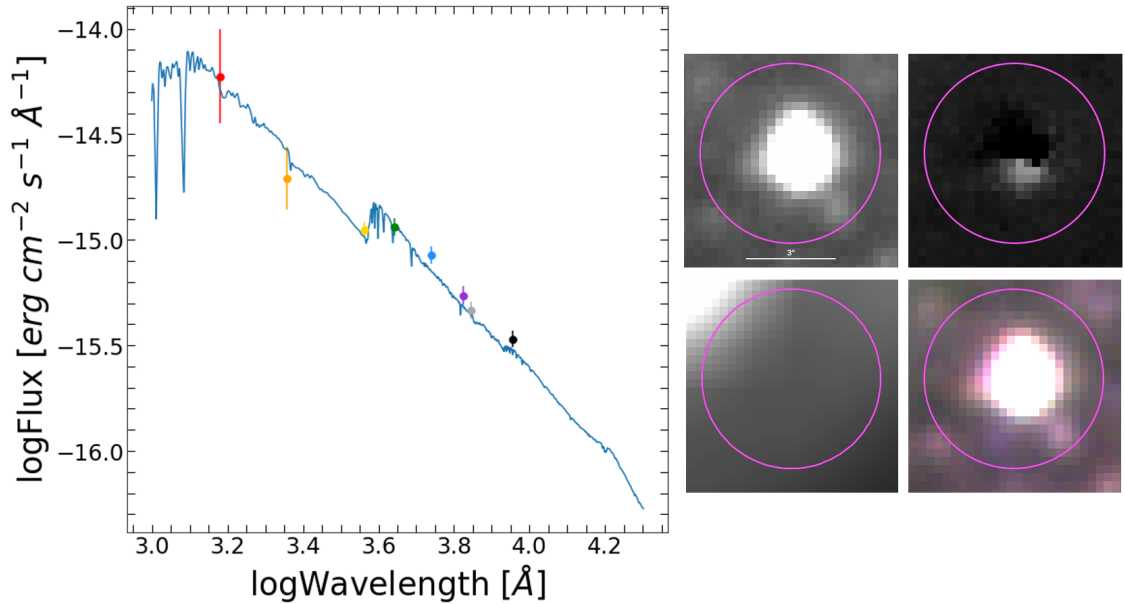


**Figure 6.** Cluster 118 is an example of a cluster with age between 10 and 100 Myr. Its best fits values are: age = 40 Myr, mass =  $11,000 M_{\odot}$ , and  $E(B-V) = 0.02$  mag. The panels, symbols, lines, and flux scales are the same as in Fig. 5.

M33 clusters, where they impose a constant value  $E(B-V)=0.1$  to derive their ages. We note this limitation, which implies that several of our clusters in the 300 Myr–1 Gyr age range could be much older than what we find.

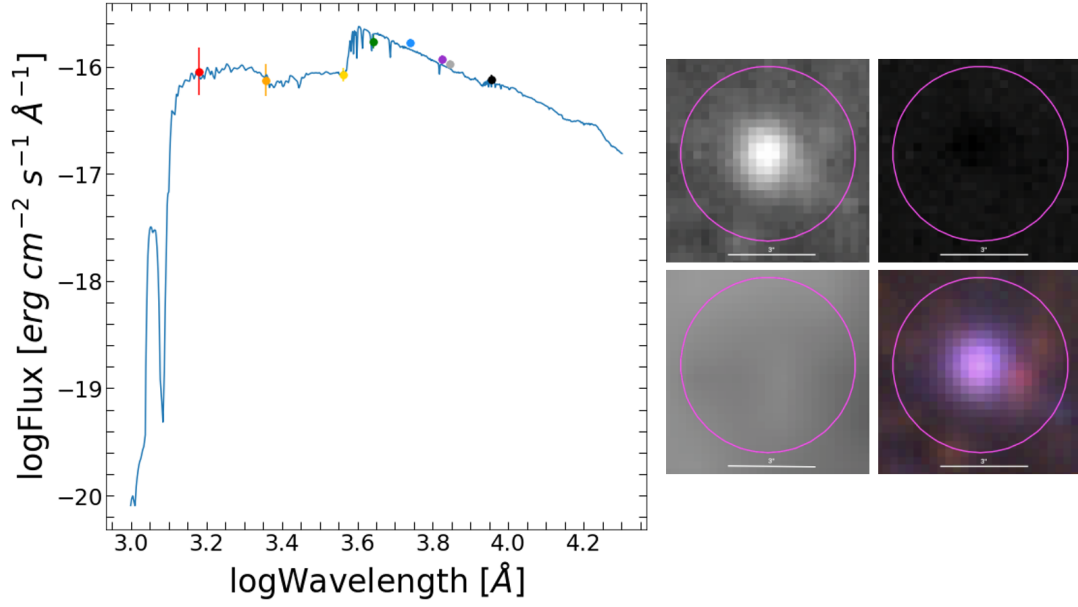


**Figure 7.** Cluster 124 is an example of a  $> 100$  Myr cluster. Its best fits values are: age = 300 Myr, mass =  $11,000 M_{\odot}$ , and  $E(B-V) = 0.1$  mag. The panels, symbols, lines, and flux scales are the same as in Fig. 5.

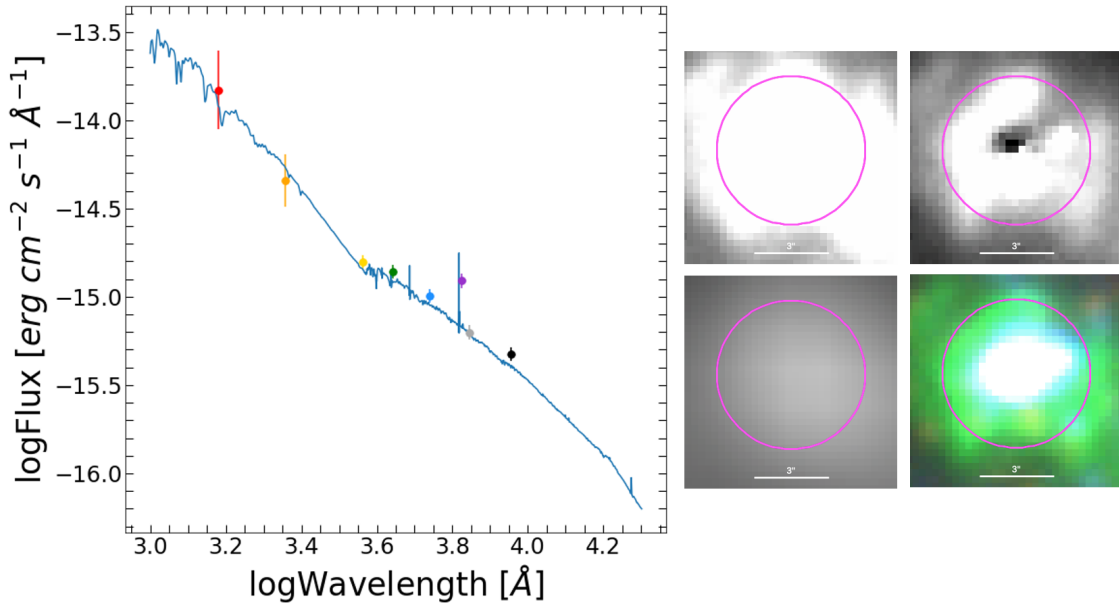


**Figure 8.** Cluster 103 is an example of a  $< 10$  Myr cluster with a large  $H\alpha$  envelope which extends outside of the photometric aperture. Some of the  $H\alpha$  emission is missed in the photometric measurements because of this, which explains some of the weakness of the  $H\alpha$  emission in the SED. This cluster has best fit age = 8 Myr, mass =  $2600 M_{\odot}$  and  $E(B-V) = 0.0$  mag. The panels, symbols, lines, and flux scales are the same as in Fig. 5.

Artificially ‘too-young’ ages produce color excess values that are unusually high, or distributions that are uncharacteristically skewed towards high values. The right panel of Figure 9 shows the distribution of the best-fit  $E(B-V)$  as a function of cluster age. The maximum  $E(B-V)$  value we recover is  $\lesssim 0.6$  mag, and  $> 2/3$  of the clusters have  $E(B-V) < 0.2$  mag, as expected for modestly reddened environments. As a reminder, the quoted values of  $E(B-V)$  include the contribution of the foreground Milky Way dust,  $E(B-V) = 0.036$  mag. The distribution is notably ‘flat’,

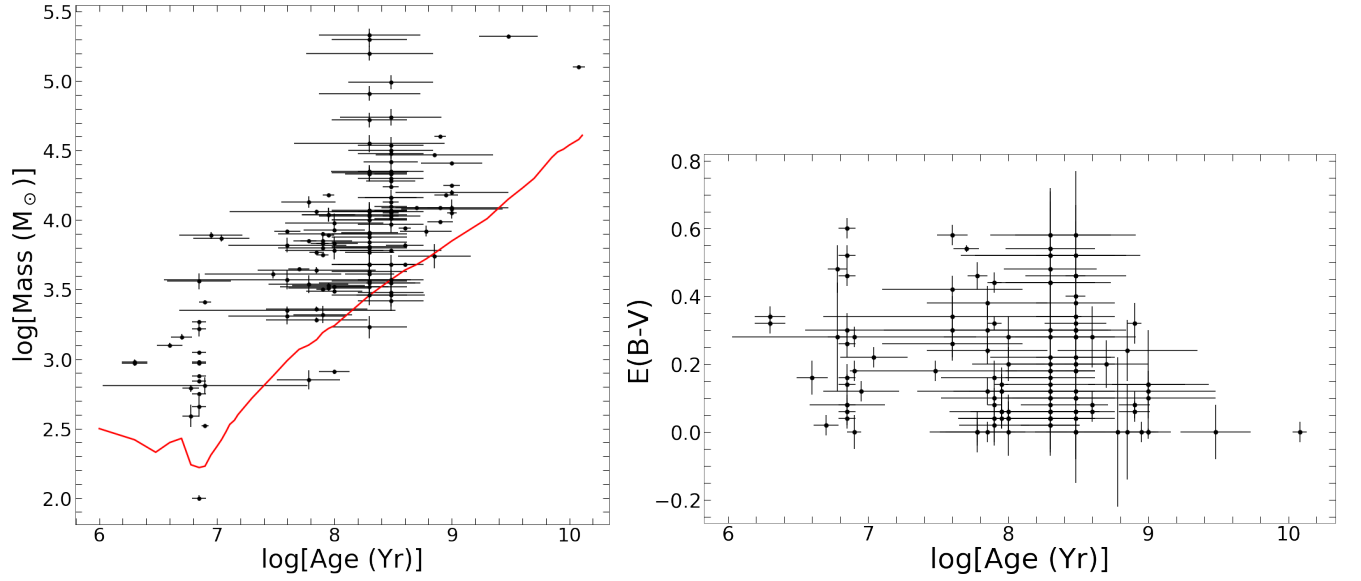


**Figure 9.** The masses (left panel) and color excesses  $E(B-V)$  (right panel) as a function age for the 137 star clusters in M33 derived via our SED fits. The red line in the left panel shows the luminosity limit of the sample.

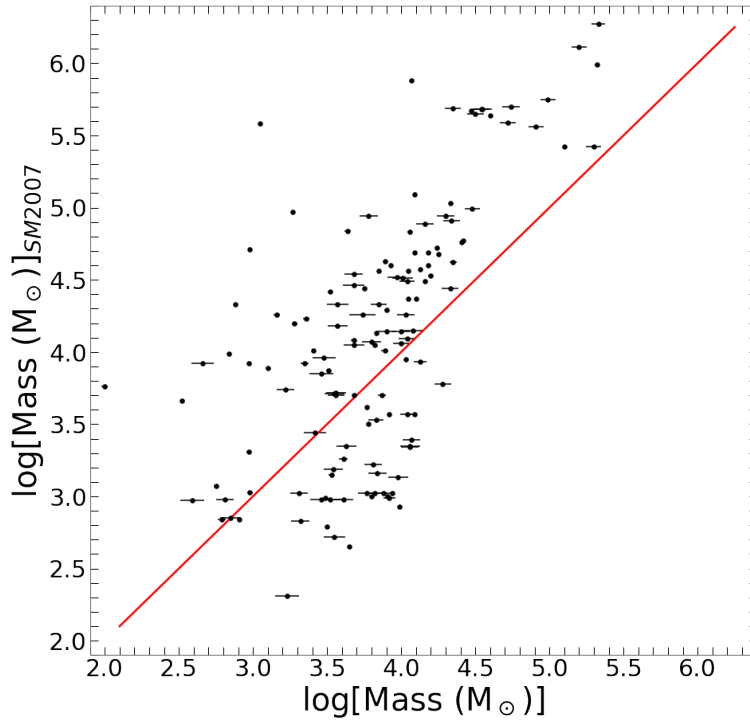


**Figure 10.** Comparison of our SED-fit masses with those of the SM2007 catalog. The 1-to-1 line is shown in red.

with several clusters yielding ages  $\geq 300$  Myr and  $E(B-V) \geq 0.4$  mag. One such cluster is shown at the top of Figure 4. In this case, the UV-optical SED are not able to provide constraints on the age-dust degeneracy, and the UV emission from the stellar population is weak, implying a weak  $24 \mu\text{m}$  dust emission. Figure 12 shows the distribution of the  $24 \mu\text{m}/\text{FUV}$  flux ratio as a function of the FUV-NUV color. The  $24 \mu\text{m}/\text{FUV}$  flux ratio measures the fraction of UV light absorbed by dust and re-emitted in the infrared; the FUV-NUV color, here given as the ratio of the flux density at the two wavelengths, measures the amount of dust reddening suffered by the UV SED (Meurer et al. 1999; Calzetti et al. 2000). The star clusters in M33 are consistent with modest-to-negligible reddening and processing of UV light

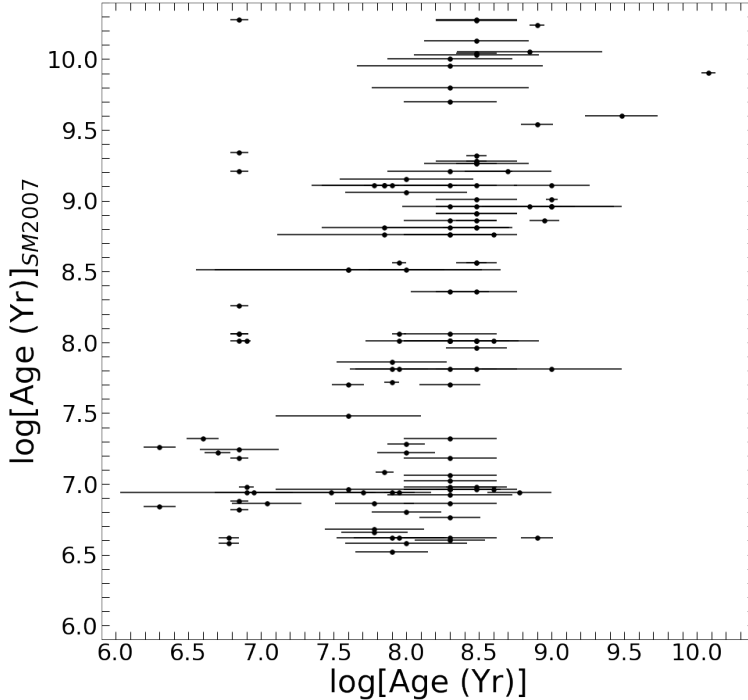


**Figure 11.** Comparison of our SED-fit ages with those of the SM2007 catalog.

into the infrared, in general agreement with our findings for the  $E(B-V)$  values. The red (more negative)  $FUV-NUV$  colors at very low values of the  $24\ \mu\text{m}/FUV$  ratio are easily explained with effects of age in the clusters SEDs (Calzetti et al. 2005; Cortese et al. 2006). From this analysis, we conclude that, while many of the clusters with ages  $\geq 300$  Myr in our sample could be older if they are less dusty than what we find from our SED fits (see discussion in Whitmore et al. 2020), the data at hand do not allow us to unequivocally conclude this. However, our age determinations for the clusters younger than  $\approx 300$  Myr are reasonably robust.

### 5.2. Colors versus Age and Extinction

The  $B-V$  color becomes redder for increasing age, as discussed by many authors, including SM2007. Our measurements follow this general trend, although we note a significant scatter towards red colors at fixed age (Figure 13). A large scatter in the direction of redder colors at fixed age is also observed for the  $NUV-I$  color, although there is still a general trend of redder colors for increasing age (Figure 14). This color, and similar colors (e.g.,  $NUV-K$ ) that use a large wavelength baseline to magnify effects, was introduced as an age indicator for galaxies once the effects of internal extinction are removed (e.g., Muñoz-Mateos et al. 2007; Cortese et al. 2008). We verify here that the same colors can be used as effective age indicators also in the case of star clusters. As already discussed by other authors, one downside of the long wavelength baseline is the sensitivity of the  $NUV-I$  color to dust extinction, as shown both by the scatter noted above (Figure 14) and by the trend of redder colors for increasing  $E(B-V)$  values we observe for our clusters (Figure 15). In this figure we show the locus of a 200 Myr star cluster for increasing values of  $E(B-V)$  as a red line. Most clusters in our sample scatter around this line, with  $< 10$  clusters deviating from this trend by showing much redder  $NUV-I$  colors.

In Figures 13 and 14 we show model expectations for both metallicities  $Z = 0.02$  (red lines) and  $Z = 0.008$  (blue lines). Notably, the differences between the two model lines are small, and well within our measurement and parameter fit uncertainties; this further justifies the use of  $Z = 0.02$  models for our SED fits. As already mentioned above, while the colors follow the general trend of the age lines, the data scatter mostly *above* these lines; this is particularly evident for the  $NUV-I$  color (Figure 14), and is the expected effect of dust extinction.

## 6. SUMMARY AND CONCLUSIONS

Leveraging the extended wavelength baseline provided by the *GALEX* UV together with optical and  $H\alpha$  bands, we have used SED-fitting to derive improved ages, masses, and extinction values for 137 confirmed star clusters in M33.

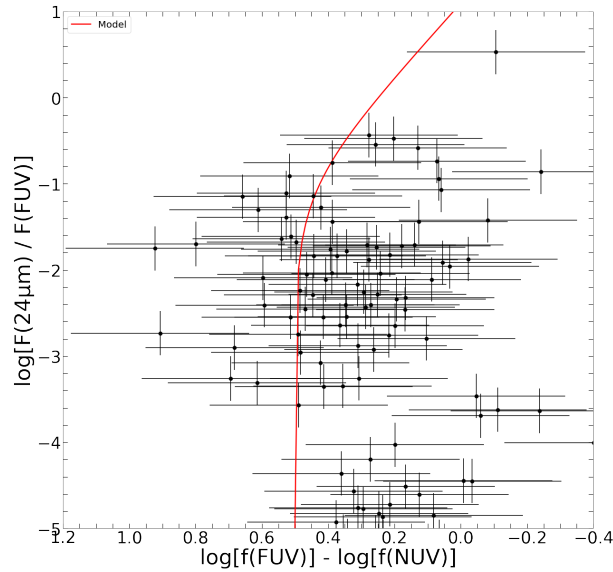


**Figure 12.** The flux ratio  $24\mu\text{m}/\text{FUV}$  plotted against flux density ratio  $\text{FUV}-\text{NUV}$ . The y-axis is the logarithm of the ratio of the two fluxes at  $24\mu\text{m}$  and FUV, expressed as  $F = \lambda f(\lambda)$  in units of  $\text{erg}/\text{cm}^2/\text{s}$ . The x-axis is the logarithm of the ratio of the flux densities in the FUV and NUV, in units of  $\text{erg}/\text{cm}^2/\text{\AA}$ . The  $24\mu\text{m}/\text{FUV}$  ratio gives a measure of the dust extinction affecting the FUV emission (Meurer et al. 1999). This correlation has been previously observed for galaxies and HII regions, and is extended here to clusters. The model line, in red, is from Calzetti et al. (2005). Most of the clusters in M33 are consistent with low-to-negligible dust attenuation. The large scatter in the FUV-NUV colors at constant  $24\mu\text{m}/\text{FUV}$  value are due to the age differences in the stellar populations of the clusters, with redder colors for older populations.

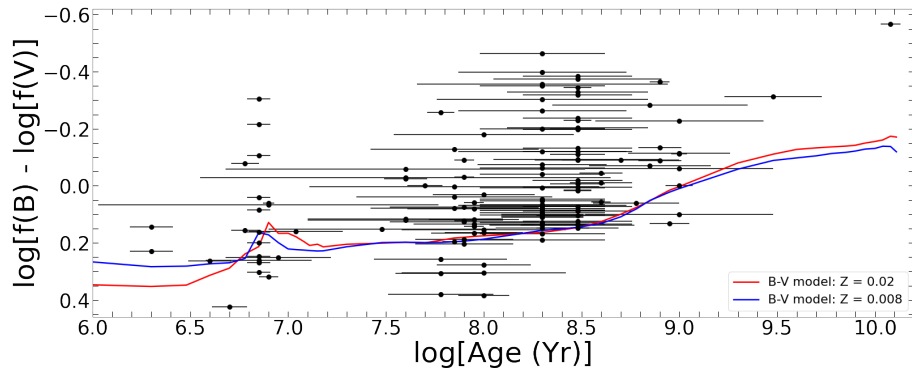


**Figure 13.** The B-V flux ratio v. age using our measurements, without any extinction correction. Correcting the flux ratio for the effect of the Milky Way foreground extinction would make it bluer (move downward) by 0.036 dex, which is significantly smaller than the scatter in the data.

Identified from the compilation of Sarajedini & Mancone (2007), all clusters also have masses and ages derived in a series of papers by Ma et al. (2001, 2002a,b,c, 2004a,b). The  $24\mu\text{m}$  emission detected by the *Spitzer Space Telescope* provides an additional discriminant for breaking the age-extinction degeneracy below 100 Myr. We exclude 26 clusters from the original list of 163 for a number of reasons that affect their SEDs, such as presence of multiple sources with different colors within the measurement aperture (Table 7). We compare our results with the earlier ones.

In terms of cluster ages, we find overall agreement with the earlier results, but also noticeable differences. About half dozen clusters that were given ages older than 100 Myr are younger than  $\sim 10$  Myr based on our method. We also find ages  $\gtrsim 100$  Myr for about a dozen clusters that were previously given ages  $\lesssim 10$  Myr. We note a dearth of clusters with ages  $> 1$  Gyr in our sample, possibly due to a well-known problem with SED fits which tend to prefer younger ages at higher extinctions over older, less extinguished solutions (Whitmore et al. 2020). As a result, we observe a clumping of clusters around  $\sim 200$ – $300$  Myr of age.

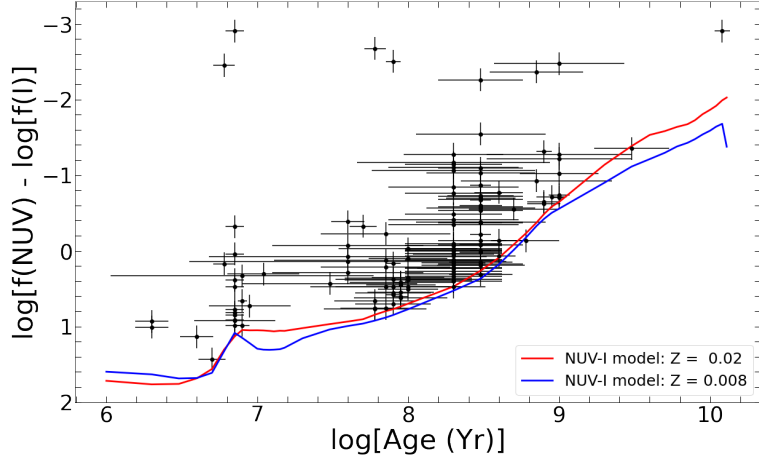


**Figure 14.** NUV-I prior to extinction corrections plotted against our calculated ages. For the FUV-I color axis, blue is down and red is up. Correction for the Milky Way foreground extinction makes the color bluer by less than 0.1 dex.

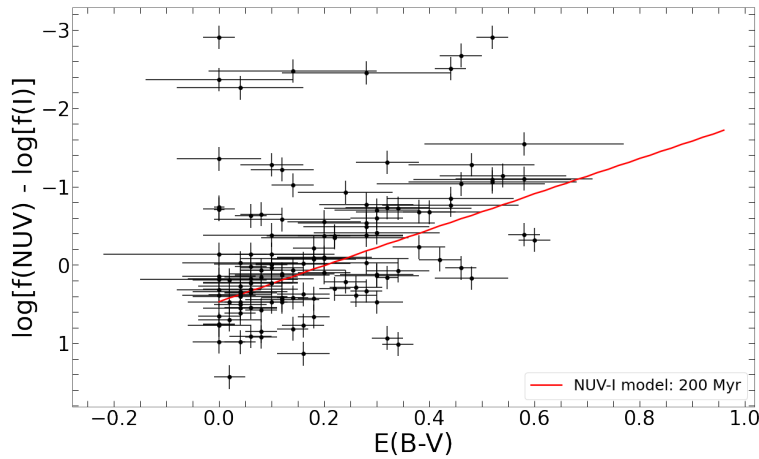


**Figure 15.** NUV-I without extinction corrections plotted against the measured  $E(B-V)$  values. The over-plotted model is set at the median age of the dataset, 200 Myr.

Unlike ages, our SED-derived masses track the earlier determinations reasonably well. The main discrepancy is that we do not find cluster masses  $\gtrsim 2 \times 10^5 M_{\odot}$ , while SM2007 reports a little over a dozen clusters above this mass. We attribute much of the discrepancy to the dearth of clusters older than  $\sim 1$  Gyr in our fits. We should remark that the mass range we find for the star clusters in M33 is consistent with the mass range found for star clusters in other spiral galaxies at comparable age intervals (Adamo & Bastian 2018).

All our star clusters have moderate-to-small internal extinction, all with  $E(B-V) < 0.6$  mag, and about 2/3 with  $E(B-V) < 0.2$  mag. We do not observe a trend between age and extinction, although the fast timescale for the diffusion of star clusters in galaxies (Grasha et al. 2017a,b) would imply that they reach regions of low dust content within several tens of Myr. Aforementioned age-extinction degeneracies for intermediate age clusters ( $\geq 200$ –300 Myr) could explain why we observe an extinction value as high as  $\sim 0.6$  mag in a  $\sim 300$  Myr old cluster; an older age with a lower extinction may be an alternate, viable explanation.

In addition to providing the list of physical parameters for the 137 clusters whose SEDs we fit, we also publish our 10-band photometry for all 163 clusters, which includes: *GALEX* FUV and NUV, optical U, B, V, R,  $H\alpha$ , and I, and infrared centered at  $3.6 \mu\text{m}$  and  $24 \mu\text{m}$ . Our photometry table can provide a resource to test alternative methods for deriving clusters' physical parameters that may overcome some of the limitations discussed in this work.



**Table 5.** Derived and literature physical properties of the M33 star clusters

SM2007	ID	RA	Dec	SM2007	Age	Age Err	SM2007	Mass	Mass Err	E(B-V)	E(B-V) Err	Comments
ID	This Work			Age			Mass					
9	0	01 32 42.93	+30 35 38.6	8.56	6.85	±0.06	4.63	3.06	±0.082	0.3	±0.08	
10	1	01 32 44.30	+30 40 12.4	10.28	6.85	±0.06	5.58	3.05	±0.025	0.6	±0.07	
16	2	01 32 52.65	+30 14 30.9	8.01	8.3	±0.32	3.72	3.56	±0.071	0.04	±0.08	
26	3	01 32 56.32	+30 14 58.9	10.04	8.48	±0.07	5.88	4.05	±0.006	0.04	±0.03	
40	4	01 33 08.11	+30 28 00.2	9.15	8.3	±0.44	4.42	3.63	±0.024	0.18	±0.08	
41	5	01 33 09.82	+30 12 50.7	7.96	8.3	±0.43	3.71	3.5	±0.08	0.06	±0.07	
42	6	01 33 10.11	+30 29 56.9	6.58	6.78	±0.07	2.97	2.57	±0.064	0.26	±0.12	
45	8	01 33 13.87	+30 29 05.1	8.96	9	±0.33	4.15	4.08	±0.006	0.14	±0.07	
49	9	01 33 14.30	+30 28 22.8	10.27	8.48	±0.28	5.68	4.54	±0.061	0.52	±0.13	
52	10	01 33 15.17	+30 32 53.0	9.11	8.6	±0.21	4.33	3.54	±0.083	0.1	±0.15	
53	11	01 33 16.10	+30 20 56.7	6.96	8.3	±0.53	3.02	3.88	±0.07	0.12	±0.08	
54	12	01 33 16.63	+30 34 35.7	8.01	8.48	±0.58	3.5	3.78	±0.008	0.28	±0.07	
68	15	01 33 22.32	+30 40 59.4	8.36	8.3	±0.24	4.08	3.66	±0.014	0.08	±0.04	
70	16	01 33 23.10	+30 33 00.5	7.86	8	±0.3	4.29	3.92	±0.015	0.06	±0.04	
74	17	01 33 23.90	+30 40 26.0	6.92	8.3	±0.54	2.72	3.53	±0.08	0.2	±0.13	
76	18	01 33 24.85	+30 33 55.0	7.28	8	±0.35	2.84	2.91	±0.029	0.04	±0.03	
77	19	01 33 25.60	+30 29 56.8	10.24	8.9	±0.11	5.64	4.6	±0.012	0.32	±0.07	
81	20	01 33 26.37	+30 41 06.9	7.7	7.6	±0.38	3.57	3.92	±0.022	0.58	±0.03	
85	22	01 33 26.75	+30 33 21.4	7.08	7.85	±0.06	3.62	3.77	±0.007	0	±0.03	
86	23	01 33 26.94	+30 34 52.6	6.94	6.9	±1.44	2.98	2.81	±0.075	0.28	±0.05	Two sources within the aperture, which appear of similar age. Log(age)=6.85 and E(B-V)=0.14 provides a comparably good fit, but absence of 24 μm emission eliminates the younger age.
87	24	01 33 27.40	+30 41 59.8	10.28	8.3	±0.64	5.69	4.35	±0.063	0.48	±0.14	One/two additional dimmer sources within aperture which do not affect photometry.
88	25	01 33 27.96	+30 37 28.4	6.86	7.78	±0.26	2.85	2.85	±0.072	0	±0.03	
91	27	01 33 28.13	+30 58 30.6	10.03	8.3	±0.76	5.7	4.71	±0.034	0.66	±0.17	
93	28	01 33 28.40	+30 36 23.1	8.76	8	±0.52	4.83	4.13	±0.02	0.26	±0.06	
101	30	01 33 30.68	+30 26 31.8	10.05	8.9	±0.43	5.67	4.46	±0.006	0.2	±0.09	
102	31	01 33 30.70	+30 22 21.4	9.28	8.48	±0.14	4.94	4.28	±0.01	0.32	±0.05	
103	32	01 33 30.90	+30 49 11.8	8.96	8.48	±0.28	4.52	3.97	±0.064	0.22	±0.09	
105	33	01 33 31.00	+30 36 52.6	6.96	7.6	±0.5	3.02	3.8	±0.055	0.24	±0.05	
106	34	01 33 31.10	+30 33 45.5	7.81	9.3	±0.35	3.57	4.16	±0.017	0	±0.07	
109	35	01 33 31.25	+30 50 07.0	7.81	8.3	±0.43	3.44	3.37	±0.083	0.12	±0.1	
110	36	01 33 31.39	+30 40 20.4	9.26	8.3	±0.97	5.03	4.32	±0.068	0.4	±0.14	
114	38	01 33 32.17	+30 40 31.9	6.52	8	±0.42	2.83	3.33	±0.075	0	±0.07	

**Table 5** continued on next page

Table 5 (continued)

SM2007 ID	ID	RA	Dec	SM2007 Age	Age	Age Err	SM2007 Mass	Mass	Mass Err	E(B-V)	E(B-V) Err	Comments
	This Work											
117	40	01 33 32.43	+30 38 24.5	9.54	8.9	$\pm 0.14$	5.09	4.09	$\pm 0.005$	0.08	$\pm 0.04$	
118	41	01 33 32.59	+30 39 24.5	8.01	8.6	$\pm 0.16$	3.7	3.68	$\pm 0.007$	0.08	$\pm 0.04$	Two sources within aperture, appear to be of similar age. Brighter source is much brighter in H $\alpha$
119	42	01 33 32.72	+30 36 55.2	6.84	6.3	$\pm 0.11$	3.03	2.96	$\pm 0.02$	0.3	$\pm 0.04$	
121	43	01 33 33.00	+30 49 41.7	9.21	8.78	$\pm 0.25$	4.69	4.07	$\pm 0.006$	0.14	$\pm 0.07$	Older best fit age retained.
122	44	01 33 33.28	+30 48 30.5	8.86	7.95	$\pm 0.48$	4.51	3.88	$\pm 0.015$	0.4	$\pm 0.07$	
124	45	01 33 33.72	+30 40 03.0	8.96	8.3	$\pm 0.33$	4.62	4.31	$\pm 0.025$	0.44	$\pm 0.1$	Contamination from a bright nearby source at H $\alpha$
126	46	01 33 34.38	+30 42 01.3	6.94	8.78	$\pm 0.25$	2.99	3.92	$\pm 0.082$	0	$\pm 0.22$	Older best fit retained
127	47	01 33 34.68	+30 48 21.2	8.51	7.6	$\pm 0.92$	3.92	3.33	$\pm 0.031$	0.32	$\pm 0.07$	
130	48	01 33 35.10	+30 49 00.0	9.9	10.08	$\pm 0.05$	5.42	5.1	$\pm 0.004$	0	$\pm 0.01$	Contamination in the UV from neighboring source
131	49	01 33 35.27	+30 33 11.6	8.01	6.9	$\pm 0.05$	3.66	2.52	$\pm 0.025$	0.18	$\pm 0.07$	Two sources within the aperture, appear to be of similar age
132	50	01 33 35.62	+30 38 36.7	6.58	8	$\pm 0.42$	3.13	3.98	$\pm 0.067$	0	$\pm 0.07$	Two sources within the aperture, appear to be of similar age
140	52	01 33 37.24	+30 34 13.9	6.94	8	$\pm 0.64$	3.57	4.04	$\pm 0.063$	0.04	$\pm 0.05$	
144	53	01 33 38.04	+30 33 05.4	7.22	8	$\pm 0.42$	3.53	3.81	$\pm 0.063$	0.02	$\pm 0.05$	
145	54	01 33 38.08	+30 33 17.6	8.96	9.3	$\pm 0.24$	4.53	4.24	$\pm 0.013$	0	$\pm 0.07$	Two sources within the aperture, appear to be of similar age
146	55	01 33 38.14	+30 42 22.9	8.26	6.85	$\pm 0.06$	3.92	2.66	$\pm 0.024$	0.3	$\pm 0.06$	Younger best fit age retained because of presence of 24 $\mu$ m emission
168	57	01 33 42.71	+30 43 49.6	8.06	6.85	$\pm 0.06$	3.99	2.82	$\pm 0.083$	0.24	$\pm 0.08$	
171	58	01 33 43.80	+30 40 56.7	7.26	6.3	$\pm 0.22$	3.31	2.95	$\pm 0.032$	0.32	$\pm 0.07$	
172	59	01 33 43.85	+30 32 10.4	8.06	6.85	$\pm 0.06$	4.33	2.88	$\pm 0.013$	0.08	$\pm 0.03$	
178	60	01 33 45.10	+30 47 46.7	9.6	9.48	$\pm 0.29$	5.99	5.32	$\pm 0.057$	0	$\pm 0.13$	Older best fit age retained
179	61	01 33 45.14	+30 49 09.2	8.81	7.95	$\pm 0.58$	4.2	3.32	$\pm 0.025$	0.2	$\pm 0.06$	
181	62	01 33 45.80	+30 27 17.3	7.18	8.3	$\pm 0.36$	3.22	3.81	$\pm 0.021$	0.16	$\pm 0.06$	
182	63	01 33 46.29	+30 47 51.0	9.28	8.48	$\pm 0.14$	4.57	4.13	$\pm 0.01$	0.4	$\pm 0.06$	
186	64	01 33 48.46	+30 45 38.7	9.11	6.85	$\pm 0.06$	4.56	3.08	$\pm 0.093$	0.56	$\pm 0.13$	
190	65	01 33 49.36	+30 47 12.5	7.02	8.3	$\pm 0.32$	3.16	3.84	$\pm 0.066$	0.06	$\pm 0.07$	
191	66	01 33 49.62	+30 34 25.7	8.06	8.3	$\pm 0.32$	4.06	4	$\pm 0.059$	0.2	$\pm 0.08$	
192	67	01 33 50.19	+30 34 18.8	8.81	8.3	$\pm 0.49$	4.26	4.01	$\pm 0.023$	0.42	$\pm 0.08$	
197	70	01 33 50.85	+30 38 34.5	7.22	6.7	$\pm 0.13$	4.26	3.16	$\pm 0.028$	0.02	$\pm 0.04$	Secondary, much dimmer source within aperture, which appears to be of similar age as primary
198	71	01 33 50.90	+30 38 55.5	6.86	7	$\pm 0.24$	3.7	3.78	$\pm 0.026$	0.18	$\pm 0.03$	
199	72	01 33 50.90	+30 +31 44.8	8.01	8.3	$\pm 0.32$	4.14	3.88	$\pm 0.065$	0.02	$\pm 0.07$	
201	73	01 33 51.24	+30 34 13.2	6.96	8.3	$\pm 0.32$	3.02	3.77	$\pm 0.066$	0.08	$\pm 0.07$	
204	74	01 33 51.80	+30 +31 47.2	8.01	6.85	$\pm 0.06$	3.76	2	$\pm 0.021$	0.06	$\pm 0.04$	

Table 5 continued on next page

Table 5 (continued)

SM2007	ID	RA	Dec	SM2007	Age	Age Err	SM2007	Mass	Mass Err	E(B-V)	E(B-V) Err	Comments
ID	This Work			Age		Mass						
206	75	01 33 52.20	+30 29 03.8	9.7	8.3	±0.32	5.59	4.7	±0.057	0.42	±0.12	
207	76	01 33 52.38	+30 35 00.8	6.98	8.3	±0.32	2.98	3.46	±0.076	0.1	±0.1	
212	77	01 33 53.40	+30 33 02.8	6.62	6.78	±0.07	2.84	2.79	±0.055	0.48	±0.11	
214	78	01 33 53.69	+30 48 21.5	7.72	7.78	±0.07	4.13	3.76	±0.011	0.1	±0.04	Older best fit age retained.
215	79	01 33 54.10	+30 33 09.7	7.32	6.6	±0.11	3.89	3.1	±0.016	0.16	±0.06	
216	80	01 33 54.38	+30 21 51.9	9.01	9	±0.11	4.56	4.07	±0.007	0.02	±0.03	
219	82	01 33 54.75	+30 45 28.4	6.62	8	±0.74	3	3.81	±0.027	0.12	±0.06	Older best fit age retained
220	83	01 33 54.80	+30 32 15.8	6.82	6.85	±0.06	3.07	2.75	±0.078	0.14	±0.06	
221	84	01 33 55.00	+30 32 14.5	6.62	8	±0.5	3.15	3.54	±0.027	0.02	±0.03	Some contamination from cluster 83; older best fit age retained
222	85	01 33 55.18	+30 47 58.0	7.7	8.3	±0.22	4.44	4.33	±0.013	0.02	±0.03	Older best fit age retained.
228	86	01 33 56.18	+30 38 39.8	6.94	6.9	±2.52	3.26	2.97	±0.078	0.2	±0.05	
229	87	01 33 56.21	+30 45 51.8	8.01	8.48	±0.29	3.85	3.46	±0.09	0	±0.15	
237	89	01 33 57.28	+30 39 15.3	9.11	7.85	±0.81	4.84	3.62	±0.032	0.1	±0.05	Older best fit age retained
238	90	01 33 57.35	+30 41 28.5	6.62	8.9	±0.11	2.93	3.99	±0.005	0.06	±0.03	
239	91	01 33 57.40	+30 52 17.9	8.01	8.3	±0.43	4.07	3.82	±0.075	0.06	±0.08	
241	93	01 33 57.84	+30 35 31.8	9.34	6.85	±0.06	4.97	3.25	±0.083	0.5	±0.1	
243	94	01 33 57.87	+30 33 25.7	7.18	6.85	±0.06	3.92	2.95	±0.006	0.02	±0.03	
245	95	01 33 58.01	+30 45 45.2	8.01	7.95	±0.22	4.49	4.04	±0.052	0.12	±0.05	
246	96	01 33 58.03	+30 39 26.2	7.24	6.85	±0.0	3.7	2.78	±0.005	0.06	±0.01	Second source within aperture, appears to be of similar age
247	97	01 33 58.10	+30 38 15.5	9.06	8	±0.42	4.94	3.76	±0.06	0.04	±0.05	
248	98	01 33 58.41	+30 39 14.9	8.86	9	±0.2	4.6	4.2	±0.026	0	±0.07	Secondary, dimmer source within aperture, with minimal impact on photometry
255	100	01 33 59.52	+30 45 49.9	6.88	6.85	±0.06	3.74	3.22	±0.066	0.16	±0.05	
257	101	01 33 59.74	+30 41 24.4	6.68	7.78	±0.34	3.19	3.54	±0.059	0	±0.06	
260	103	01 34 00.01	+30 33 54.3	6.98	6.9	±0.05	4.01	3.41	±0.02	0	±0.07	Older best fit age retained.
264	104	01 34 00.47	+30 41 23.1	9.11	9	±0.3	4.76	4.43	±0.006	0.16	±0.06	
267	105	01 34 01.31	+30 39 23.5	6.6	8.3	±0.25	3	3.91	±0.017	0.1	±0.03	Secondary source at edge of aperture, appears to be of similar age
271	106	01 34 01.75	+30 32 25.7	8.51	7.6	±0.39	4.18	3.55	±0.065	0.28	±0.05	Second source within aperture, appear to be of similar age; younger best fit age retained
272	107	01 34 01.99	+30 38 10.9	6.62	8.3	±0.32	2.98	3.5	±0.085	0.02	±0.1	
273	108	01 34 01.99	+30 39 37.8	9.8	8.3	±0.97	6.11	5.18	±0.056	0.5	±0.15	
275	109	01 34 02.48	+30 40 40.7	9.11	8.3	±0.86	5.42	5.26	±0.063	0.5	±0.16	
281	110	01 34 02.90	+30 43 20.8	9.21	8.3	±0.64	5.56	4.89	±0.062	0.28	±0.14	
282	111	01 34 03.09	+30 45 35.6	9.21	6.85	±0.06	4.71	2.98	±0.091	0.46	±0.09	
284	112	01 34 03.12	+30 52 13.9	6.98	8.3	±0.22	3.78	4.23	±0.013	0.06	±0.03	
289	113	01 34 03.90	+30 47 29.1	7.06	8.3	±0.43	3.39	4.07	±0.064	0.14	±0.09	

Table 5 continued on next page

Table 5 (continued)

SM2007	ID	RA	Dec	SM2007	Age	Age Err	SM2007	Mass	Mass Err	E(B-V)	E(B-V) Err	Comments
ID	This Work			Age		Mass	Mass					
316	117	01 34 08.04	+30 38 38.2	10	8.3	$\pm 0.53$	6.27	5.31	$\pm 0.051$	0.56	$\pm 0.1$	
320	118	01 34 08.53	+30 39 02.4	6.66	7.6	$\pm 0.34$	3.93	4.05	$\pm 0.046$	0.02	$\pm 0.03$	
322	120	01 34 08.70	+30 42 55.3	8.36	8.48	$\pm 0.28$	3.96	3.48	$\pm 0.084$	0.04	$\pm 0.1$	
327	121	01 34 09.71	+30 21 30.0	6.76	8.3	$\pm 0.26$	2.98	3.61	$\pm 0.022$	0.02	$\pm 0.03$	
329	122	01 34 10.09	+30 45 29.4	6.96	8.3	$\pm 0.43$	3.35	4.03	$\pm 0.08$	0.2	$\pm 0.12$	
333	123	01 34 11.00	+30 40 30.1	8.81	8.3	$\pm 0.43$	4.77	4.39	$\pm 0.069$	0.38	$\pm 0.15$	
335	124	01 34 11.35	+30 41 27.9	8.56	8.48	$\pm 0.14$	4.37	4.05	$\pm 0.006$	0.1	$\pm 0.03$	
338	125	01 34 11.82	+30 42 19.9	8.91	8.3	$\pm 0.04$	4.46	3.65	$\pm 0.043$	0.18	$\pm 0.09$	
345	126	01 34 13.84	+30 19 47.3	8.86	8.3	$\pm 0.26$	4.54	3.66	$\pm 0.02$	0.16	$\pm 0.04$	
347	127	01 34 14.02	+30 39 29.5	8.01	8.48	$\pm 0.14$	3.95	4.03	$\pm 0.008$	0.18	$\pm 0.04$	
350	128	01 34 14.20	+30 39 58.4	8.96	9	$\pm 0.15$	4.68	4.27	$\pm 0.009$	0.02	$\pm 0.06$	
351	129	01 34 14.65	+30 32 35.0	8.56	8.48	$\pm 0.29$	4.37	4.1	$\pm 0.014$	0.2	$\pm 0.05$	
353	130	01 34 15.04	+30 41 19.2	6.96	8.3	$\pm 0.32$	3.34	4.06	$\pm 0.061$	0.06	$\pm 0.07$	
355	131	01 34 15.51	+30 42 11.5	8.51	8.3	$\pm 0.13$	4.6	4.05	$\pm 0.009$	0.1	$\pm 0.05$	
359	132	01 34 16.38	+30 37 49.1	7.81	8.3	$\pm 0.26$	4.09	4.04	$\pm 0.016$	0.04	$\pm 0.03$	
360	133	01 34 16.57	+30 40 29.0	8.96	8.85	$\pm 0.31$	4.26	3.74	$\pm 0.077$	0	$\pm 0.11$	
361	134	01 34 17.54	+30 42 36.7	7.48	7.6	$\pm 1.05$	3.02	3.31	$\pm 0.068$	0.42	$\pm 0.06$	
371	136	01 34 19.89	+30 36 12.7	7.81	7.9	$\pm 0.25$	4.33	3.85	$\pm 0.056$	0.02	$\pm 0.05$	
372	137	01 34 20.17	+30 39 33.3	6.96	8.6	$\pm 0.11$	3.02	3.94	$\pm 0.006$	0.06	$\pm 0.03$	
376	139	01 34 21.59	+30 36 45.6	7.81	7.9	$\pm 0.38$	3.87	3.48	$\pm 0.016$	0.12	$\pm 0.05$	Younger best fit age retained
377	140	01 34 21.99	+30 44 39.1	7.32	8.3	$\pm 0.32$	3.35	3.61	$\pm 0.067$	0.04	$\pm 0.07$	Two/three sources within aperture, which appear to be of similar age
383	141	01 34 23.13	+30 43 46.4	6.94	7.9	$\pm 0.05$	2.79	3.48	$\pm 0.014$	0.3	$\pm 0.04$	Older best fit age retained.
384	142	01 34 23.52	+30 25 58.2	8.01	8.3	$\pm 0.32$	4.14	4	$\pm 0.065$	0.12	$\pm 0.07$	
385	143	01 34 24.53	+30 53 05.4	10.13	8.3	$\pm 0.97$	5.65	4.47	$\pm 0.068$	0.54	$\pm 0.18$	
387	144	01 34 25.40	+30 41 28.4	9.01	8.3	$\pm 0.43$	4.99	4.47	$\pm 0.066$	0.38	$\pm 0.14$	
392	145	01 34 27.10	+30 36 42.3	8.91	8.3	$\pm 0.43$	4.89	4.13	$\pm 0.069$	0.18	$\pm 0.1$	
400	147	01 34 29.10	+30 53 20.6	8.81	8.48	$\pm 0.36$	4.49	4.14	$\pm 0.012$	0.3	$\pm 0.07$	
406	148	01 34 31.74	+30 39 14.8	9.11	7.9	$\pm 0.05$	4.23	3.37	$\pm 0.026$	0.34	$\pm 0.06$	Older best fit age retained
409	149	01 34 32.90	+30 38 12.0	9.11	7.85	$\pm 0.06$	4.44	3.7	$\pm 0.011$	0.44	$\pm 0.03$	Older best fit age retained.
410	150	01 34 33.09	+30 37 36.3	6.8	8	$\pm 0.24$	2.99	3.49	$\pm 0.015$	0.04	$\pm 0.03$	
411	151	01 34 33.12	+30 38 14.2	8.76	8.6	$\pm 0.43$	4.05	3.82	$\pm 0.017$	0.28	$\pm 0.08$	
412	152	01 34 33.19	+30 38 26.6	8.76	8.3	$\pm 0.54$	4.05	3.66	$\pm 0.08$	0.26	$\pm 0.13$	
416	154	01 34 35.30	+30 38 30.1	9.32	8.48	$\pm 0.14$	4.72	4.22	$\pm 0.006$	0.44	$\pm 0.04$	
420	156	01 34 40.41	+30 46 01.3	6.94	6.95	$\pm 0.27$	4.01	3.89	$\pm 0.03$	0.12	$\pm 0.06$	
422	157	01 34 40.72	+30 53 02.0	6.94	7.7	$\pm 0.26$	2.65	3.65	$\pm 0.014$	0.54	$\pm 0.03$	
427	158	01 34 43.70	+30 47 37.9	8.76	8.3	$\pm 0.32$	4.91	4.34	$\pm 0.059$	0.18	$\pm 0.09$	
428	159	01 34 44.20	+30 52 18.9	9.95	8.3	$\pm 1.08$	5.68	4.53	$\pm 0.069$	0.5	$\pm 0.19$	
432	160	01 34 45.91	+30 53 04.4	6.86	8.3	$\pm 0.32$	2.31	3.21	$\pm 0.09$	0.1	$\pm 0.13$	

Table 5 continued on next page

Table 5 (*continued*)

SM2007	ID	RA	Dec	SM2007	Age	Age Err	SM2007	Mass	Mass Err	E(B-V)	E(B-V) Err	Comments
ID	This Work			Age			Mass					
438	161	01 34 49.62	+30 21 55.5	9.26	8.48	$\pm 0.57$	5.75	4.97	$\pm 0.052$	0.28	$\pm 0.11$	
439	162	01 34 50.10	+30 47 04.1	8.06	7.85	$\pm 0.06$	4.69	4.14	$\pm 0.008$	0.1	$\pm 0.03$	Older best fit age retained.

NOTE—SED-fitting derived ages, masses, and colors excesses, E(B-V); together with 1  $\sigma$  uncertainties for 137 confirmed star clusters in M33, listed together with the ages and masses compiled in Sarajedini & Mancone (2007), indicated as SM2007. The E(B-V) values in this Table are the sum of the internal dust reddening in the star cluster plus the foreground reddening of the Milky Way, E(B-V)=0.036 (Schlafly & Finkbeiner 2011). In some instances of two or more sources present in the aperture, the best fit results are retained if the sources appear of comparable age (similar behavior in colors), as indicated in the Comments field; in this case, the quoted mass is the sum of all masses for the sources in the aperture. For sources yielding with two best-fits to the age/extinction, the reported value reflects an assessment based on the 24  $\mu\text{m}$  emission. The retained best fit is given in the Comments field.

Table 6. Photometric measurements of the M33 star clusters

ID	ID	f(FUV)	f(NUV)	f(U)	f(B)	f(V)	f(R)	f(H $\alpha$ )	f(I)	F(3.6 $\mu$ m)	F(24 $\mu$ m)
SM2007	This Work	erg/s/cm <sup>2</sup> /Å	erg/s/cm <sup>2</sup> /Å	erg/s/cm <sup>2</sup> /Å	erg/s/cm <sup>2</sup> /Å	erg/s/cm <sup>2</sup> /Å	erg/s/cm <sup>2</sup> /Å	erg/s/cm <sup>2</sup> /Å	erg/s/cm <sup>2</sup> /Å	erg/s/cm <sup>2</sup>	erg/s/cm <sup>2</sup>
9	0	4.43E-16	2.79E-16	1.52E-16	2.48E-16	2.34E-16	1.54E-16	2.01E-16	1.07E-16	1.56E-13	<4.3E-16
10	1	2.88E-17	2.54E-17	2.4E-17	5.09E-17	6.9E-17	5.84E-17	6.91E-17	5.29E-17	8.79E-14	2.67E-15
16	2	1.4E-16	7.83E-17	6.34E-17	1.01E-16	9.39E-17	5.81E-17	6.4E-17	3.6E-17	2.67E-14	5.55E-15
26	3	1.63E-16	9.12E-17	1.37E-16	2.4E-16	2.2E-16	1.35E-16	1.49E-16	8.72E-17	5.63E-14	<4.3E-16
40	4	5.17E-17	2.89E-17	2.62E-17	4.9E-17	5.87E-17	4.32E-17	4.51E-17	3.09E-17	3.36E-14	7.23E-15
41	5	1.06E-16	4.19E-17	6.11E-17	1.04E-16	8.96E-17	5.48E-17	5.25E-17	2.99E-17	1.4E-14	6.27E-15
42	6	<7.8E-19	<9.4E-19	7.48E-17	1.06E-16	9.07E-17	5.73E-17	1.26E-16	3.66E-17	3.47E-15	6.63E-14
44	7	3.66E-17	<9.4E-19	2.06E-17	5.33E-17	7.64E-17	6.73E-17	7.36E-17	5.66E-17	5.06E-14	9.85E-15
45	8	<7.8E-19	<9.4E-19	1.93E-17	4.45E-17	5.59E-17	4.62E-17	5.36E-17	3.86E-17	5.37E-14	9.58E-15
49	9	6.27E-18	7.21E-18	4E-17	8.65E-17	1.27E-16	1.11E-16	1.29E-16	8.94E-17	1.11E-13	<4.3E-16
52	10	9.37E-18	1.64E-17	1.7E-17	3.03E-17	3.46E-17	2.72E-17	3.87E-17	1.98E-17	3.31E-13	9.88E-15
53	11	1.43E-16	8.2E-17	9.64E-17	1.55E-16	1.45E-16	9.1E-17	1.06E-16	6.25E-17	7.1E-14	9.96E-15
54	12	<7.8E-19	1.12E-17	1.86E-17	3.86E-17	4.23E-17	3.5E-17	3.59E-17	2.69E-17	3.11E-14	<4.3E-16
66	13	2.82E-16	1.07E-16	1.41E-16	1.78E-16	1.83E-16	1.46E-16	1.8E-16	1.43E-16	3.56E-13	<4.3E-16
67	14	1.96E-16	7.74E-17	1.33E-16	1.78E-16	1.68E-16	1.17E-16	1.41E-16	1.04E-16	2.42E-13	1.25E-14
68	15	1.55E-16	4.49E-17	6.54E-17	1.04E-16	9.05E-17	5.52E-17	5.62E-17	4.1E-17	5.53E-14	2.71E-14
70	16	8.72E-16	3.79E-16	2.47E-16	3.36E-16	2.96E-16	1.87E-16	2.19E-16	1.28E-16	1.54E-13	1.53E-14
74	17	4.12E-17	1.05E-17	2.82E-17	4.32E-17	4.03E-17	2.39E-17	4.06E-17	2.35E-17	2.37E-14	2.55E-15
76	18	1.1E-16	3.99E-17	3.72E-17	4.3E-17	2.93E-17	1.64E-17	1.74E-17	1.33E-17	4.23E-14	1.22E-14
77	19	9.48E-19	4.79E-18	4.39E-17	9.66E-17	1.39E-16	1.22E-16	1.41E-16	9.8E-17	1.2E-13	4.41E-15
81	20	<7.8E-19	2.87E-17	3.45E-17	6.6E-17	6.77E-17	5.6E-17	6.09E-17	6.97E-17	9.62E-14	1.44E-14
83	21	4E-17	4.14E-17	2.05E-17	2.49E-16	4.19E-17	3E-17	2.2E-17	3.06E-17	4.07E-14	<4.3E-16
85	22	1.99E-15	7.7E-16	3.62E-16	4.21E-16	3.46E-16	2.07E-16	2.43E-16	1.34E-16	1.72E-13	6.73E-15
86	23	2.57E-16	1.32E-16	7.57E-17	1.08E-16	1.01E-16	7.59E-17	8.39E-17	6.15E-17	8.11E-14	1.09E-14
87	24	1.3E-17	1.67E-17	4.58E-17	7.7E-17	1.06E-16	9.33E-17	1.04E-16	7.99E-17	2.52E-13	3.36E-13
88	25	3.28E-16	8.04E-17	6.08E-17	7.17E-17	4.9E-17	2.96E-17	3.27E-17	1.77E-17	1.63E-14	1.22E-15
90	26	2.78E-17	6.19E-17	1.72E-16	2.63E-16	2.3E-16	1.34E-16	1.53E-16	8.54E-17	6.56E-14	2.95E-15
91	27	9.11E-18	3.47E-18	5.04E-17	1.17E-16	1.7E-16	1.37E-16	1.8E-16	1.22E-16	1.56E-13	3.7E-15
93	28	1.89E-16	1.75E-16	1.32E-16	2.52E-16	2.51E-16	1.74E-16	1.88E-16	1.31E-16	2.4E-13	1.59E-14
94	29	2.58E-16	2.12E-16	1.76E-16	2.79E-16	2.47E-16	1.6E-16	1.81E-16	1.06E-16	7.43E-14	3.9E-15
101	30	<7.8E-19	1.1E-17	4.2E-17	9.95E-17	1.32E-16	1.09E-16	1.24E-16	9.28E-17	4.08E-13	9.55E-15
102	31	2.18E-17	1.46E-17	5.23E-17	1.08E-16	1.37E-16	1.07E-16	1.18E-16	7.69E-17	7.94E-14	3.17E-15
103	32	2.7E-17	2.02E-17	3.93E-17	8.38E-17	9.45E-17	6.47E-17	7.74E-17	4.74E-17	4.51E-14	7.51E-15
105	33	4.2E-16	2.23E-16	1.61E-16	2.13E-16	1.89E-16	1.32E-16	1.54E-16	1.15E-16	3.01E-13	4.24E-14
106	34	<7.8E-19	2.32E-18	6.05E-17	1.16E-16	1.05E-16	6.59E-17	6.24E-17	4.39E-17	4.32E-14	2.64E-14
109	35	<7.8E-19	2.91E-17	2.49E-17	4.65E-17	4.07E-17	2.89E-17	3.41E-17	1.94E-17	1.63E-14	2.56E-15
110	36	3.05E-17	2.27E-17	6.13E-17	1.31E-16	1.6E-16	1.15E-16	1.24E-16	8.99E-17	3.17E-13	6.1E-14

Table 6 continued on next page

Table 6 (continued)

ID	ID	f(FUV)	f(NUV)	f(U)	f(B)	f(V)	f(R)	f(H $\alpha$ )	f(I)	F(3.6 $\mu$ m)	F(24 $\mu$ m)
SM2007	This Work	$\text{erg/s/cm}^2/\text{\AA}$	$\text{erg/s/cm}^2/\text{\AA}$	$\text{erg/s/cm}^2/\text{\AA}$	$\text{erg/s/cm}^2/\text{\AA}$	$\text{erg/s/cm}^2/\text{\AA}$	$\text{erg/s/cm}^2/\text{\AA}$	$\text{erg/s/cm}^2/\text{\AA}$	$\text{erg/s/cm}^2/\text{\AA}$	$\text{erg/s/cm}^2$	$\text{erg/s/cm}^2$
113	37	1.64E-15	4.97E-16	3.67E-16	4.47E-16	3.77E-16	2.49E-16	2.67E-16	1.68E-16	1.79E-13	3.25E-15
114	38	4.22E-16	1.37E-16	1.02E-16	1.18E-16	9.63E-17	5.38E-17	7.35E-17	3.82E-17	2.48E-14	5.79E-15
116	39	5.4E-18	2.45E-17	1.39E-17	3.27E-17	4.26E-17	4.75E-17	6.13E-17	6.13E-17	1.25E-13	<4.3E-16
117	40	<7.8E-19	1.18E-17	3.72E-17	8.06E-17	9.21E-17	6.68E-17	7.31E-17	5.24E-17	8.71E-14	2.98E-14
118	41	1.29E-17	3.27E-17	3.28E-17	5.64E-17	5.9E-17	3.53E-17	4.04E-17	2.81E-17	1.97E-14	<4.3E-16
119	42	1.28E-15	4.58E-16	2.76E-16	2.04E-16	1.62E-16	1.31E-16	1.21E-15	5.35E-17	2.83E-13	7.05E-13
121	43	<7.8E-19	1.42E-17	3.4E-17	7.7E-17	8.43E-17	6.1E-17	6.96E-17	5.06E-17	2.32E-14	2.32E-14
122	44	4.39E-17	4.65E-17	4.21E-17	8.79E-17	9.81E-17	6.91E-17	9.39E-17	5.73E-17	7.52E-14	4.51E-15
124	45	3.59E-17	4.3E-18	5.63E-17	1.17E-16	1.26E-16	9.31E-17	1.13E-16	8.14E-17	1.09E-13	4.87E-15
126	46	6.22E-18	3.6E-17	8.38E-17	1.02E-16	9.6E-17	6.69E-17	1.93E-16	4.91E-17	9.02E-14	1.9E-13
127	47	7.59E-17	3.87E-17	2.94E-17	4.78E-17	5.07E-17	3.72E-17	4.47E-17	3.28E-17	4.88E-14	<4.3E-16
130	48	<7.8E-19	<9.4E-19	2.1E-17	7.03E-17	1.24E-16	1.15E-16	1.44E-16	1.04E-16	1.94E-13	<4.3E-16
131	49	2.81E-16	1.81E-16	4.66E-17	7.88E-17	7.41E-17	5.63E-17	4.78E-17	3.97E-17	1.15E-13	9.79E-15
132	50	2.06E-15	4.17E-16	8.47E-16	8.51E-16	6.27E-16	3.14E-16	3.99E-16	1.72E-16	9.35E-15	8.66E-15
134	51	3.46E-16	2.4E-16	1.45E-16	2.26E-16	2.17E-16	1.49E-16	1.79E-16	1.19E-16	1.63E-13	1.84E-15
140	52	1.42E-15	6.26E-16	3.86E-16	5.27E-16	4.46E-16	2.74E-16	2.96E-16	1.79E-16	2.1E-13	4.88E-15
144	53	1.03E-15	3.55E-16	2.7E-16	3.37E-16	2.86E-16	1.67E-16	1.92E-16	1.11E-16	2.38E-13	<4.3E-16
145	54	<7.8E-19	3.2E-18	5.53E-17	1.12E-16	1.19E-16	8.07E-17	8.56E-17	5.29E-17	6.23E-14	<4.3E-16
146	55	1.44E-16	1.26E-16	6.33E-17	9.06E-17	8.32E-17	5.07E-17	6.87E-17	4.24E-17	7.96E-14	9.34E-14
153	56	8.13E-16	2.86E-16	1.07E-16	9.56E-17	7.28E-17	4.55E-17	1.87E-16	5E-17	1.82E-13	2.43E-13
168	57	5.08E-16	1.73E-16	1.15E-16	1.48E-16	1.42E-16	9.79E-17	1.32E-16	7.14E-17	7.14E-14	1.37E-14
171	58	9.23E-16	5.11E-16	1.79E-16	1.42E-16	1.23E-16	1.09E-16	1.35E-15	4.99E-17	2.67E-13	2.03E-12
172	59	2.31E-15	8.34E-16	3.93E-16	4.61E-16	3.52E-16	2.05E-16	2.72E-16	1.19E-16	5.5E-14	9.05E-14
178	60	<7.8E-19	2.05E-17	2.53E-16	5.32E-16	7.28E-16	5.86E-16	7.23E-16	4.62E-16	4.99E-13	2.35E-15
179	61	6.69E-17	4.1E-17	3.05E-17	4.93E-17	4.56E-17	2.92E-17	3.71E-17	2.49E-17	6.52E-14	<4.3E-16
181	62	9.06E-17	4.73E-17	6.17E-17	1.11E-16	1.06E-16	6.76E-17	7.31E-17	4.9E-17	6.4E-14	1.36E-14
182	63	5.5E-18	9.57E-18	2.33E-17	5.22E-17	6.57E-17	5.32E-17	6.65E-17	4.51E-17	7.14E-14	<4.3E-16
186	64	3.69E-17	<9.4E-19	3.68E-17	7.97E-17	1.03E-16	7.45E-17	8.65E-17	6.1E-17	5.6E-14	<4.3E-16
190	65	2.23E-16	1.09E-16	1.21E-16	1.83E-16	1.6E-16	9.67E-17	1.18E-16	6.56E-17	4.2E-14	1.16E-14
191	66	9.41E-17	5.5E-17	6.75E-17	1.41E-16	1.4E-16	9.52E-17	1.01E-16	6.89E-17	1.22E-13	<4.3E-16
192	67	1.47E-17	6.05E-18	2.95E-17	5.4E-17	6.09E-17	4.96E-17	5.01E-17	4.25E-17	7.83E-14	1.98E-14
194	68	1.07E-15	1.37E-16	2.4E-16	3.18E-16	2.6E-16	1.39E-16	1.87E-16	9.38E-17	7.26E-14	1.39E-16
195	69	1.58E-16	8.62E-17	6.55E-18	1.77E-17	2.45E-17	2.65E-17	2.52E-17	3.24E-17	9.71E-14	1.64E-14
197	70	1.32E-14	4.32E-15	1.57E-15	1.29E-15	8.44E-16	3.75E-16	4.26E-16	1.6E-16	1.55E-13	2.72E-14
198	71	5.13E-15	1.07E-15	9.22E-16	8.51E-16	7.25E-16	5.04E-16	6.11E-16	5.3E-16	1.17E-12	4.93E-14
199	72	3.92E-16	1.45E-16	1.4E-16	2.06E-16	1.9E-16	1.22E-16	1.39E-16	7.83E-17	3.32E-14	<4.3E-16
201	73	1.86E-16	7.65E-17	7.79E-17	1.28E-16	1.15E-16	7.29E-17	7.91E-17	5.35E-17	9E-14	5.14E-14
204	74	3.23E-16	1.32E-16	6.28E-17	7.37E-17	6.04E-17	3.15E-17	3.95E-17	1.62E-17	1.46E-14	2.29E-14
206	75	7.36E-17	3.62E-17	1.01E-16	2.22E-16	3.15E-16	2.7E-16	3.09E-16	2.09E-16	2.48E-13	<4.3E-16

Table 6 continued on next page

Table 6 (continued)

ID	ID	f(FUV)	f(NUV)	f(U)	f(B)	f(V)	f(R)	f(H $\alpha$ )	f(I)	F(3.6 $\mu$ m)	F(24 $\mu$ m)
SM2007	This Work	$\text{erg/s/cm}^2/\text{\AA}$	$\text{erg/s/cm}^2/\text{\AA}$	$\text{erg/s/cm}^2/\text{\AA}$	$\text{erg/s/cm}^2/\text{\AA}$	$\text{erg/s/cm}^2/\text{\AA}$	$\text{erg/s/cm}^2/\text{\AA}$	$\text{erg/s/cm}^2/\text{\AA}$	$\text{erg/s/cm}^2/\text{\AA}$	$\text{erg/s/cm}^2$	$\text{erg/s/cm}^2$
207	76	7.6E-17	2.43E-17	4.69E-17	6.47E-17	5.35E-17	3.36E-17	4.89E-17	2.48E-17	3.46E-14	1.23E-14
212	77	6.27E-17	5.41E-17	4.05E-17	5.17E-17	5.59E-17	4.44E-17	9.11E-17	3.66E-17	5.52E-14	5.49E-14
214	78	7.99E-16	4.28E-16	2.09E-16	2.94E-16	2.6E-16	1.62E-16	2.01E-16	1.13E-16	1.06E-13	2.39E-14
215	79	4.93E-15	1.47E-15	8.61E-16	6.68E-16	5.13E-16	3.21E-16	1.78E-15	1.08E-16	3.55E-13	2.96E-12
216	80	<7.8E-19	9.76E-18	4.21E-17	8.63E-17	9.65E-17	6.65E-17	7.61E-17	4.97E-17	4.51E-14	<4.3E-16
217	81	1.48E-16	1.8E-16	3.94E-17	6.32E-17	6.65E-17	5.83E-17	9.96E-17	3.94E-17	5.19E-13	2.42E-13
219	82	3.93E-16	2.09E-16	1.13E-16	2.08E-16	1.93E-16	1.26E-16	1.41E-16	8.79E-17	5.18E-14	1.11E-12
220	83	8.03E-16	4.91E-16	1.77E-16	2.61E-16	2.22E-16	1.29E-16	1.62E-16	7.53E-17	5.88E-14	1.07E-14
221	84	5.35E-16	2.44E-16	1.23E-16	1.92E-16	1.68E-16	1.02E-16	1.25E-16	5.9E-17	2.31E-14	1.17E-14
222	85	9.84E-16	6.69E-16	4.02E-16	6.16E-16	5.52E-16	3.37E-16	4.03E-16	2.23E-16	1.98E-13	2.62E-14
228	86	8.47E-16	2.93E-16	1.99E-16	2.19E-16	1.88E-16	1.28E-16	1.55E-16	1.09E-16	1.58E-13	5.73E-14
229	87	6.05E-17	3.81E-17	4.84E-17	6.83E-17	5.95E-17	3.4E-17	7.17E-17	2.47E-17	7.83E-14	1.55E-13
231	88	4.93E-17	3.35E-17	9.41E-17	2.1E-16	2.69E-16	2.07E-16	2.36E-16	1.54E-16	1.26E-13	<4.3E-16
237	89	5.5E-16	2.23E-16	1.27E-16	1.81E-16	1.74E-16	9.7E-17	1.25E-16	7.51E-17	1.23E-13	7.36E-14
238	90	<7.8E-19	1.03E-17	3.36E-17	6.42E-17	7.01E-17	4.9E-17	5.94E-17	4.35E-17	2.69E-14	<4.3E-16
239	91	1.83E-16	1.59E-16	1.18E-16	2.06E-16	1.74E-16	1.02E-16	1.18E-16	6.28E-17	4.26E-14	<4.3E-16
240	92	1.1E-16	2.6E-17	2.82E-17	4.97E-17	4.83E-17	3.38E-17	4.15E-17	3.77E-17	1.34E-13	<4.3E-16
241	93	9.25E-17	<9.4E-19	6.17E-17	1.29E-16	1.6E-16	1.26E-16	1.63E-16	1.04E-16	1.2E-13	1.93E-13
243	94	4.74E-15	1.56E-15	6.21E-16	6E-16	4.43E-16	2.53E-16	3.04E-16	1.61E-16	2.22E-13	3.98E-14
245	95	7.11E-16	4.36E-16	2.71E-16	4.13E-16	3.67E-16	2.26E-16	2.67E-16	1.56E-16	1.35E-13	8.17E-14
246	96	1.79E-15	8.09E-16	3.72E-16	3.75E-16	2.89E-16	1.6E-16	1.87E-16	9.7E-17	8.36E-14	5.41E-14
247	97	9.38E-16	2.12E-16	2.11E-16	2.46E-16	2.11E-16	1.34E-16	1.36E-16	9.27E-17	1.7E-13	<4.3E-16
248	98	<7.8E-19	1.37E-17	1.07E-16	1.62E-16	1.42E-16	8.59E-17	9.5E-17	7.09E-17	1.75E-13	<4.3E-16
250	99	8.25E-16	4.91E-16	1.47E-16	1.94E-16	1.76E-16	1.16E-16	1.07E-16	9.16E-17	1.54E-13	1.73E-13
255	100	2.01E-15	1.28E-15	6.17E-16	6.94E-16	5.42E-16	3.14E-16	3.97E-16	2.15E-16	3.24E-13	3.46E-14
257	101	1.13E-15	5.13E-16	4.51E-16	4.19E-16	3.24E-16	1.67E-16	2.21E-16	8.71E-17	9.32E-15	1.43E-13
258	102	3.67E-16	2.35E-16	4.58E-17	5.3E-17	6.77E-17	6.18E-17	6.23E-17	7.04E-17	1.33E-13	1.02E-14
260	103	1.48E-14	4.55E-15	1.57E-15	1.39E-15	1.01E-15	6.28E-16	1.23E-15	4.73E-16	1.45E-12	3.22E-13
264	104	<7.8E-19	7.92E-18	4.99E-17	1E-16	1.12E-16	9.32E-17	1.12E-16	8.26E-17	2.08E-13	<4.3E-16
267	105	1.67E-16	1.21E-16	1.12E-16	1.74E-16	1.5E-16	8.49E-17	1.01E-16	7.1E-17	5.2E-14	2.5E-14
271	106	1.79E-16	8.12E-17	5.96E-17	9.92E-17	1.02E-16	7.2E-17	7.99E-17	5.91E-17	1.01E-13	<4.3E-16
272	107	1.94E-16	3.1E-17	7.9E-17	1.23E-16	1.11E-16	5.99E-17	8.41E-17	3.3E-17	3.69E-14	2.97E-14
273	108	1.08E-16	4.56E-17	2.69E-16	5.61E-16	7.6E-16	6.09E-16	7.33E-16	5.23E-16	5.57E-13	<4.3E-16
275	109	1.5E-16	4.58E-17	1.75E-16	4.3E-16	6.84E-16	6.26E-16	7.64E-16	6.34E-16	1.12E-12	1.42E-13
281	110	3.66E-16	1.71E-16	2.87E-16	5.6E-16	7.29E-16	5.68E-16	6.93E-16	4.42E-16	4.81E-13	<4.3E-16
282	111	8.28E-17	6.79E-17	4.92E-17	8.02E-17	8.91E-17	7.45E-17	9.18E-17	6.2E-17	1.08E-13	4.92E-15
284	112	4.83E-16	3.35E-16	2.77E-16	4.74E-16	4.27E-16	2.55E-16	3.01E-16	1.62E-16	1.27E-13	<4.3E-16
289	113	1.83E-16	1.07E-16	1.14E-16	1.99E-16	1.86E-16	1.22E-16	1.47E-16	9.18E-17	1.18E-13	<4.3E-16
300	114	1.54E-16	5.65E-17	5.54E-17	4.57E-15	5.82E-15	1.18E-16	6.22E-15	5.68E-17	1.59E-13	8.91E-14

Table 6 continued on next page



Table 6 (continued)

ID	ID	f(FUV)	f(NUV)	f(U)	f(B)	f(V)	f(R)	f(H $\alpha$ )	f(I)	F(3.6 $\mu$ m)	F(24 $\mu$ m)
SM2007	This Work	$\text{erg/s/cm}^2/\text{\AA}$	$\text{erg/s/cm}^2/\text{\AA}$	$\text{erg/s/cm}^2/\text{\AA}$	$\text{erg/s/cm}^2/\text{\AA}$	$\text{erg/s/cm}^2/\text{\AA}$	$\text{erg/s/cm}^2/\text{\AA}$	$\text{erg/s/cm}^2/\text{\AA}$	$\text{erg/s/cm}^2/\text{\AA}$	$\text{erg/s/cm}^2$	$\text{erg/s/cm}^2$
301	115	1.72E-16	9.21E-17	5.74E-17	5.66E-15	6.35E-15	1.07E-16	1.26E-16	6.38E-17	2.47E-13	<4.3E-16
310	116	1.78E-16	9.57E-17	5.61E-17	8.84E-17	8.94E-17	6.92E-17	6.99E-17	5.44E-17	1.12E-13	<4.3E-16
316	117	8.53E-17	4.84E-17	2.08E-16	4.94E-16	7.36E-16	6.17E-16	7.42E-16	6.12E-16	8.53E-13	<4.3E-16
320	118	5.94E-15	1.96E-15	1.11E-15	1.15E-15	8.46E-16	4.64E-16	5.45E-16	3.39E-16	3.70E-13	2.61E-13
321	119	9.59E-16	4.15E-16	1.87E-16	2.8E-16	2.7E-16	1.67E-16	2.47E-16	1.1E-16	1.03E-13	3.09E-13
322	120	3.78E-17	<9.4E-19	3.61E-17	7.38E-17	6.87E-17	3.89E-17	5.37E-17	2.35E-17	4.27E-14	<4.3E-16
327	121	2.53E-16	6.52E-17	8.26E-17	1.25E-16	1.13E-16	6.71E-17	6.74E-17	4.2E-17	3.3E-14	7.57E-15
329	122	1.57E-16	1.95E-17	1.16E-16	2.12E-16	1.94E-16	1.15E-16	1.34E-16	7.42E-17	5.21E-14	2.22E-15
333	123	4.71E-17	2.25E-17	9.82E-17	2.02E-16	2.06E-16	1.42E-16	1.64E-16	1.12E-16	2.29E-13	<4.3E-16
335	124	8.99E-17	7.46E-17	8.38E-17	1.7E-16	1.67E-16	1.05E-16	1.16E-16	7.58E-17	1.15E-13	<4.3E-16
338	125	6.04E-17	1.33E-17	5.49E-17	8.57E-17	7.57E-17	4.22E-17	6.07E-17	3.21E-17	6.97E-14	3.29E-14
345	126	6.81E-17	2.89E-17	4.06E-17	6.9E-17	6.54E-17	4.49E-17	4.64E-17	3.43E-17	1.95E-13	7.62E-15
347	127	3.57E-17	3.65E-17	7.03E-17	1.28E-16	1.26E-16	8.08E-17	9.14E-17	5.99E-17	6.05E-14	<4.3E-16
350	128	<7.8E-19	1.45E-17	7.9E-17	1.59E-16	1.59E-16	1.04E-16	1.15E-16	7.96E-17	2.57E-13	6.58E-15
351	129	4.17E-17	2.86E-17	7.56E-17	1.49E-16	1.5E-16	9.8E-17	1.02E-16	6.72E-17	1.08E-13	<4.3E-16
353	130	4.23E-16	1.85E-16	1.78E-16	2.88E-16	2.62E-16	1.62E-16	1.92E-16	1.08E-16	8.33E-14	<4.3E-16
355	131	3.15E-16	1.2E-16	1.3E-16	1.93E-16	1.87E-16	1.25E-16	1.53E-16	9.61E-17	2.13E-13	2.02E-15
359	132	<7.8E-19	2.57E-16	2.06E-16	2.82E-16	2.48E-16	1.53E-16	1.66E-16	1.08E-16	1.05E-13	<4.3E-16
360	133	<7.8E-19	<9.4E-19	2.74E-17	5.79E-17	6.21E-17	4.27E-17	5.3E-17	3E-17	3.15E-14	9.04E-15
361	134	2.5E-17	2.13E-17	2.02E-17	3.47E-17	3.09E-17	2.54E-17	2.96E-17	2.49E-17	6.43E-14	3.51E-14
367	135	<7.8E-19	1.83E-16	1.77E-17	4.86E-17	8.09E-17	8.16E-17	8.64E-17	8.23E-17	1.57E-13	<4.3E-16
371	136	1.4E-15	6.9E-16	3.6E-16	4.75E-16	3.94E-16	2.33E-16	2.65E-16	1.37E-16	6.11E-14	5.9E-15
372	137	3.6E-17	3.92E-17	7.08E-17	1.29E-16	1.22E-16	7.78E-17	9.24E-17	5.36E-17	6.38E-14	<4.3E-16
375	138	<7.8E-19	1.85E-18	2.04E-17	4.4E-17	5.19E-17	4.14E-17	5.42E-17	4.03E-17	5.86E-14	1.51E-14
376	139	2.51E-16	1.23E-16	7.4E-17	1.16E-16	1.07E-16	7.05E-17	7.82E-17	4.67E-17	5.78E-14	2.53E-15
377	140	1.59E-16	8.27E-17	7.16E-17	1.08E-16	9.97E-17	5.66E-17	6.88E-17	4.08E-17	4.75E-14	4.5E-15
383	141	3.7E-17	4.48E-17	2.5E-17	4.29E-17	4.42E-17	3.54E-17	4.11E-17	3.08E-17	5.77E-14	1.06E-14
384	142	2.02E-16	1.11E-16	1.23E-16	2.17E-16	1.99E-16	1.3E-16	1.37E-16	8.28E-17	4.67E-14	1.84E-15
385	143	1.36E-17	8.65E-18	4.21E-17	9.64E-17	1.34E-16	1.12E-16	1.32E-16	9.34E-17	1.04E-13	<4.3E-16
387	144	5.18E-17	3.9E-17	9.2E-17	1.97E-16	2.4E-16	1.74E-16	2.1E-16	1.33E-16	1.69E-13	<4.3E-16
392	145	1.59E-16	7.07E-17	1.27E-16	2.24E-16	2.23E-16	1.48E-16	1.66E-16	9.71E-17	9.62E-14	<4.3E-16
399	146	1.49E-18	5.04E-18	4.89E-17	6.54E-17	7.12E-17	5.16E-17	7.55E-17	4.16E-17	5.06E-14	1.65E-15
400	147	2.01E-17	1.08E-17	4.36E-17	9.68E-17	1.06E-16	7.79E-17	8.84E-17	5.81E-17	1.75E-13	<4.3E-16
406	148	2.93E-17	1.28E-17	1.83E-17	2.65E-17	3.01E-17	2.48E-17	2.79E-17	2.16E-17	7.27E-14	<4.3E-16
409	149	2.29E-17	<9.4E-19	2.36E-17	5.18E-17	5.67E-17	4.6E-17	5.43E-17	4.13E-17	1.13E-13	<4.3E-16
410	150	4.64E-16	1.13E-16	1.33E-16	1.78E-16	1.35E-16	7.51E-17	8.29E-17	5.01E-17	5.08E-14	<4.3E-16
411	151	3.69E-18	4.11E-18	2.13E-17	4.94E-17	4.99E-17	3.65E-17	3.81E-17	2.44E-17	3.84E-14	<4.3E-16
412	152	3.63E-17	8.89E-18	2.11E-17	3.35E-17	4.09E-17	3.15E-17	3.79E-17	2.72E-17	7.91E-14	1.38E-14
413	153	2.13E-16	4.5E-17	9.22E-17	1.38E-16	1.24E-16	8.27E-17	5.69E-16	7.33E-17	1.93E-13	1.02E-14

Table 6 continued on next page

Table 6 (continued)

ID	ID	f(FUV)	f(NUV)	f(U)	f(B)	f(V)	f(R)	f(H $\alpha$ )	f(I)	F(3.6 $\mu$ m)	F(24 $\mu$ m)
SM2007	This Work	$\text{erg/s/cm}^2/\text{\AA}$	$\text{erg/s/cm}^2/\text{\AA}$	$\text{erg/s/cm}^2/\text{\AA}$	$\text{erg/s/cm}^2/\text{\AA}$	$\text{erg/s/cm}^2/\text{\AA}$	$\text{erg/s/cm}^2/\text{\AA}$	$\text{erg/s/cm}^2/\text{\AA}$	$\text{erg/s/cm}^2/\text{\AA}$	$\text{erg/s/cm}^2$	$\text{erg/s/cm}^2$
416	154	5.35E-18	6.94E-18	2.15E-17	5.48E-17	7.73E-17	6.46E-17	4.93E-17	5.14E-17	4.9E-14	<4.3E-16
419	155	1.98E-16	7.72E-17	1.14E-16	1.24E-16	1.35E-16	1.08E-16	1.35E-16	9.42E-17	1.27E-13	7.44E-15
420	156	1.24E-14	4.8E-15	1.47E-15	1.39E-15	1.08E-15	7.11E-16	8.89E-16	8.99E-16	1.62E-12	2.7E-13
422	157	<7.8E-19	1.65E-17	2.11E-17	3.89E-17	3.89E-17	3.17E-17	3.37E-17	3.49E-17	2.19E-13	1.07E-14
427	158	2.48E-16	1.7E-16	1.6E-16	3.13E-16	3.26E-16	2.16E-16	2.68E-16	1.58E-16	3.21E-13	9.01E-15
428	159	2.68E-17	8.04E-18	5.7E-17	1.26E-16	1.8E-16	1.49E-16	1.81E-16	1.18E-16	1.25E-13	8.36E-15
432	160	4.55E-17	1.4E-17	1.47E-17	2.79E-17	2.97E-17	2.25E-17	2.55E-17	1.39E-17	1.14E-14	8.48E-15
438	161	1.44E-16	1.14E-16	3.39E-16	6.39E-16	7.83E-16	6.21E-16	7.08E-16	4.18E-16	4.13E-13	1.77E-15
439	162	1.55E-15	9.81E-16	4.64E-16	7.2E-16	6.25E-16	3.98E-16	4.53E-16	2.46E-16	2.3E-13	<4.3E-16

NOTE—Photometry in 10 bands for 163 confirmed M33 star clusters in the compilation of Sarajedini & Mancone (2007). The values for the U, B, V, R, H $\alpha$ , and I bands are flux densities in units of  $\text{erg s}^{-1} \text{cm}^{-2} \text{\AA}^{-1}$ , while the values for the IR bands, 3.6  $\mu$ m and 24  $\mu$ m, are fluxes in units of  $\text{erg s}^{-1} \text{cm}^{-2}$ . The flux densities for the UV and optical bands are reported as directly measured, i.e., no correction for the foreground Milky Way extinction has been applied. Uncertainties on the measurements are listed in Table 3

Table 7. Clusters excluded from analysis.

SM2007 ID	Cluster ID	RA	Dec	SM2007 Age	SM2007 Mass	Reason for Exclusion
44	7	01 33 13.80	+30 29 03.6	10.06	5.32	Three sources within aperture, inspection of these sources shows they have different ages (brightest at different wavelengths).
66	13	01 33 22.11	+30 40 28.4	9.11	4.73	Two-three sources within aperture, inspection of these sources shows they have different ages.
67	14	01 33 22.16	+30 40 26.0	6.94	3.04	Secondary source within aperture of different age.
83	21	01 33 26.49	+30 41 11.6	6.6	2.62	Source is dim, SED data is unusual and noisy.
90	26	01 33 28.00	+30 21 06.2	6.84	2.91	Multiple sources within aperture of different ages.
94	29	01 33 28.70	+30 36 37.5	8.01	4.35	Multiple sources within aperture of different ages.
113	37	01 33 32.01	+30 33 21.8	6.98	3.54	Multiple sources within aperture of different ages.
116	39	01 33 32.36	+30 38 28.0	9.95	5.25	Source is dim, secondary source in the aperture, and bleeding from nearby sources.
134	51	01 33 36.19	+30 47 55.1	8.66	4.4	Multiple sources within aperture of different ages, as well as contamination from nearby sources.
153	56	01 33 39.71	+30 32 29.2	7.12	3.16	Multiple sources within aperture of different ages and some bleeding from nearby sources.
194	68	01 33 50.70	+30 58 50.3	7.28	3.69	Unusual SED, particularly in the UV bands.
195	69	01 33 50.73	+30 44 56.2	7.81	3.61	Unusual SED, possibly due to a nearby fainter source.
217	81	01 33 54.63	+30 34 48.3	6.94	2.86	Unusual SED.
231	88	01 33 56.50	+30 36 10.6	9.3	5.04	Multiple sources within aperture of different ages
240	92	01 33 57.66	+30 41 32.6	8.06	3.74	Unusual SED.
250	99	01 33 58.86	+30 34 43.2	8.01	3.72	Multiple sources within aperture of different ages.
258	102	01 33 59.84	+30 39 45.4	8.01	3.89	Secondary source at edge of aperture of different age
300	114	01 34 06.30	+30 37 26.1	9.16	4.97	Two sources within aperture, with different ages.
301	115	01 34 06.40	+30 37 30.5	9.16	4.89	Multiple sources within aperture of different ages
310	116	01 34 07.28	+30 38 29.5	8.01	3.81	Second source within aperture of different age.
321	119	01 34 08.63	+30 39 22.8	8.31	4.59	Multiple sources within as well as at the edge of the aperture of different ages
367	135	01 34 18.59	+30 44 47.8	10.3	5.57	Unusual SED.
375	138	01 34 21.43	+30 39 40.2	10.28	5.34	Second source within aperture of different age.
399	146	01 34 29.07	+30 38 05.4	8.61	4.1	Multiple sources within aperture of different ages
413	153	01 34 33.73	+30 39 15.7	9.11	4.76	Multiple sources within aperture of different ages
419	155	01 34 38.90	+30 38 51.8	9.01	4.6	Two sources within aperture, with different ages.

## REFERENCES

- Adamo, A., & Bastian, N. 2018, *The Lifecycle of Clusters in Galaxies*, ed. S. Stahler, Vol. 424, 91, doi: [10.1007/978-3-319-22801-3\\_4](https://doi.org/10.1007/978-3-319-22801-3_4)
- Adamo, A., Ryon, J. E., Messa, M., et al. 2017, *ApJ*, 841, 131, doi: [10.3847/1538-4357/aa7132](https://doi.org/10.3847/1538-4357/aa7132)
- Adamo, A., Zeidler, P., Kruijssen, J. M. D., et al. 2020, *SSRv*, 216, 69, doi: [10.1007/s11214-020-00690-x](https://doi.org/10.1007/s11214-020-00690-x)
- Asplund, M., Grevesse, N., Sauval, A. J., & Scott, P. 2009, *ARA&A*, 47, 481, doi: [10.1146/annurev.astro.46.060407.145222](https://doi.org/10.1146/annurev.astro.46.060407.145222)
- Ballesteros-Paredes, J., André, P., Hennebelle, P., et al. 2020, *SSRv*, 216, 76, doi: [10.1007/s11214-020-00698-3](https://doi.org/10.1007/s11214-020-00698-3)
- Bastian, N. 2008, *Monthly Notices of the Royal Astronomical Society*, 390
- Bastian, N., Adamo, A., Gieles, M., et al. 2012, *MNRAS*, 419, 2606, doi: [10.1111/j.1365-2966.2011.19909.x](https://doi.org/10.1111/j.1365-2966.2011.19909.x)
- Boquien, M., Calzetti, D., Kennicutt, R., et al. 2009, *ApJ*, 706, 553, doi: [10.1088/0004-637X/706/1/553](https://doi.org/10.1088/0004-637X/706/1/553)
- Bresolin, F. 2011, *ApJ*, 730, 129, doi: [10.1088/0004-637X/730/2/129](https://doi.org/10.1088/0004-637X/730/2/129)
- Bressert, E., Bastian, N., Gutermuth, R., et al. 2010, *MNRAS*, 409, L54, doi: [10.1111/j.1745-3933.2010.00946.x](https://doi.org/10.1111/j.1745-3933.2010.00946.x)
- Brown, G., & Gnedin, O. Y. 2021, arXiv e-prints, arXiv:2106.12420. <https://arxiv.org/abs/2106.12420>
- Bruzual, G., & Charlot, S. 1993, *ApJ*, 405, 538, doi: [10.1086/172385](https://doi.org/10.1086/172385)
- . 2003, *MNRAS*, 344, 1000, doi: [10.1046/j.1365-8711.2003.06897.x](https://doi.org/10.1046/j.1365-8711.2003.06897.x)
- Calzetti, D. 2013, *Star Formation Rate Indicators*, ed. J. Falcón-Barroso & J. H. Knapen, 419
- Calzetti, D., Armus, L., Bohlin, R. C., et al. 2000, *ApJ*, 533, 682, doi: [10.1086/308692](https://doi.org/10.1086/308692)
- Calzetti, D., Kennicutt, R. C., J., Bianchi, L., et al. 2005, *ApJ*, 633, 871, doi: [10.1086/466518](https://doi.org/10.1086/466518)
- Calzetti, D., Kennicutt, R. C., Engelbracht, C. W., et al. 2007, *ApJ*, 666, 870, doi: [10.1086/520082](https://doi.org/10.1086/520082)
- Calzetti, D., Lee, J. C., Sabbi, E., et al. 2015, *AJ*, 149, 51, doi: [10.1088/0004-6256/149/2/51](https://doi.org/10.1088/0004-6256/149/2/51)
- Calzetti, D., Battisti, A. J., Shivaee, I., et al. 2021, *ApJ*, 913, 37, doi: [10.3847/1538-4357/abf118](https://doi.org/10.3847/1538-4357/abf118)
- Cerviño, M., Valls-Gabaud, D., Luridiana, V., & Mas-Hesse, J. M. 2002, *A&A*, 381, 51, doi: [10.1051/0004-6361:20011266](https://doi.org/10.1051/0004-6361:20011266)
- Chandar, R., Bianchi, L., & Ford, H. C. 1999, *ApJ*, 517, 668, doi: [10.1086/307228](https://doi.org/10.1086/307228)
- Chandar, R., Whitmore, B. C., Dinino, D., et al. 2016, *ApJ*, 824, 71, doi: [10.3847/0004-637X/824/2/71](https://doi.org/10.3847/0004-637X/824/2/71)
- Cortese, L., Gavazzi, G., & Boselli, A. 2008, *MNRAS*, 390, 1282, doi: [10.1111/j.1365-2966.2008.13838.x](https://doi.org/10.1111/j.1365-2966.2008.13838.x)
- Cortese, L., Boselli, A., Buat, V., et al. 2006, *ApJ*, 637, 242, doi: [10.1086/498296](https://doi.org/10.1086/498296)
- Crowther, P. A., Schnurr, O., Hirschi, R., et al. 2010, *MNRAS*, 408, 731, doi: [10.1111/j.1365-2966.2010.17167.x](https://doi.org/10.1111/j.1365-2966.2010.17167.x)
- Dale, D. A., Cohen, S. A., Johnson, L. C., et al. 2009, *ApJ*, 703, 517, doi: [10.1088/0004-637X/703/1/517](https://doi.org/10.1088/0004-637X/703/1/517)
- de Grijs, R., Anders, P., Lamers, H. J. G. L. M., et al. 2005, *MNRAS*, 359, 874, doi: [10.1111/j.1365-2966.2005.08914.x](https://doi.org/10.1111/j.1365-2966.2005.08914.x)
- Draine, B. T., & Li, A. 2007, *ApJ*, 657, 810, doi: [10.1086/511055](https://doi.org/10.1086/511055)
- Eldridge, J. J., Stanway, E. R., Xiao, L., et al. 2017, *PASA*, 34, e058, doi: [10.1017/pasa.2017.51](https://doi.org/10.1017/pasa.2017.51)
- Elmegreen, B. 2003, in *IAU Joint Discussion*, Vol. 25, IAU Joint Discussion, E34
- Elmegreen, B. G. 2010, in *Star Clusters: Basic Galactic Building Blocks Throughout Time and Space*, ed. R. de Grijs & J. R. D. Lépine, Vol. 266, 3–13, doi: [10.1017/S1743921309990809](https://doi.org/10.1017/S1743921309990809)
- Elmegreen, B. G., & Efremov, Y. N. 1997, *ApJ*, 480, 235, doi: [10.1086/303966](https://doi.org/10.1086/303966)
- Fazio, G. G., Hora, J. L., Allen, L. E., et al. 2004, *ApJS*, 154, 10, doi: [10.1086/422843](https://doi.org/10.1086/422843)
- Ferrarese, L., Mould, J. R., Kennicutt, Robert C., J., et al. 2000, *ApJ*, 529, 745, doi: [10.1086/308309](https://doi.org/10.1086/308309)
- Fitzpatrick, E. L. 1999, *PASP*, 111, 63, doi: [10.1086/316293](https://doi.org/10.1086/316293)
- Gieles, M. 2009, *MNRAS*, 394, 2113, doi: [10.1111/j.1365-2966.2009.14473.x](https://doi.org/10.1111/j.1365-2966.2009.14473.x)
- Gieles, M., & Bastian, N. 2008, *A&A*, 482, 165, doi: [10.1051/0004-6361:20078909](https://doi.org/10.1051/0004-6361:20078909)
- Gieles, M., Larsen, S. S., Bastian, N., & Stein, I. T. 2006a, *A&A*, 450, 129, doi: [10.1051/0004-6361:20053589](https://doi.org/10.1051/0004-6361:20053589)
- Gieles, M., Portegies Zwart, S. F., Baumgardt, H., et al. 2006b, *MNRAS*, 371, 793, doi: [10.1111/j.1365-2966.2006.10711.x](https://doi.org/10.1111/j.1365-2966.2006.10711.x)
- Girardi, L., Bressan, A., Bertelli, G., & Chiosi, C. 2000, *A&AS*, 141, 371, doi: [10.1051/aas:2000126](https://doi.org/10.1051/aas:2000126)
- Grasha, K., Calzetti, D., Adamo, A., et al. 2015, *ApJ*, 815, 93, doi: [10.1088/0004-637X/815/2/93](https://doi.org/10.1088/0004-637X/815/2/93)
- . 2017a, *ApJ*, 840, 113, doi: [10.3847/1538-4357/aa6f15](https://doi.org/10.3847/1538-4357/aa6f15)
- Grasha, K., Elmegreen, B. G., Calzetti, D., et al. 2017b, *ApJ*, 842, 25, doi: [10.3847/1538-4357/aa740b](https://doi.org/10.3847/1538-4357/aa740b)
- Gutkin, J., Charlot, S., & Bruzual, G. 2016, *MNRAS*, 462, 1757, doi: [10.1093/mnras/stw1716](https://doi.org/10.1093/mnras/stw1716)
- Helou, G., Roussel, H., Appleton, P., et al. 2004, *ApJS*, 154, 253, doi: [10.1086/422640](https://doi.org/10.1086/422640)
- Hunter, D. A., Elmegreen, B. G., Dupuy, T. J., & Mortonson, M. 2003, *AJ*, 126, 1836, doi: [10.1086/378056](https://doi.org/10.1086/378056)
- Iglesias, C. A., Rogers, F. J., & Wilson, B. G. 1992, *ApJ*, 397, 717, doi: [10.1086/171827](https://doi.org/10.1086/171827)

- Johnson, L. C., Seth, A. C., Dalcanton, J. J., et al. 2017, *ApJ*, 839, 78, doi: [10.3847/1538-4357/aa6alf](https://doi.org/10.3847/1538-4357/aa6alf)
- Kennicutt, Robert C., J., Lee, J. C., Funes, J. G., et al. 2008, *ApJS*, 178, 247, doi: [10.1086/590058](https://doi.org/10.1086/590058)
- Kennicutt, R. C., & Evans, N. J. 2012, *ARA&A*, 50, 531, doi: [10.1146/annurev-astro-081811-125610](https://doi.org/10.1146/annurev-astro-081811-125610)
- Kong, X., Zhou, X., Chen, J., et al. 2000, *AJ*, 119, 2745, doi: [10.1086/301396](https://doi.org/10.1086/301396)
- Kroupa, P. 2001, *MNRAS*, 322, 231, doi: [10.1046/j.1365-8711.2001.04022.x](https://doi.org/10.1046/j.1365-8711.2001.04022.x)
- Krumholz, M. R., Adamo, A., Fumagalli, M., & Calzetti, D. 2019a, *MNRAS*, 482, 3550, doi: [10.1093/mnras/sty2896](https://doi.org/10.1093/mnras/sty2896)
- Krumholz, M. R., McKee, C. F., & Bland-Hawthorn, J. 2019b, *ARA&A*, 57, 227, doi: [10.1146/annurev-astro-091918-104430](https://doi.org/10.1146/annurev-astro-091918-104430)
- Krumholz, M. R., Adamo, A., Fumagalli, M., et al. 2015, *ApJ*, 812, 147, doi: [10.1088/0004-637X/812/2/147](https://doi.org/10.1088/0004-637X/812/2/147)
- Lada, C., & Lada, E. 2003, *ARAA*, 41
- Larsen, S. S. 2002, *AJ*, 124, 1393, doi: [10.1086/342381](https://doi.org/10.1086/342381)
- . 2009, *A&A*, 494, 539, doi: [10.1051/0004-6361:200811212](https://doi.org/10.1051/0004-6361:200811212)
- Leitherer, C., Schaerer, D., Goldader, J. D., et al. 1999, *ApJS*, 123, 3, doi: [10.1086/313233](https://doi.org/10.1086/313233)
- Li, H., Gnedin, O. Y., & Gnedin, N. Y. 2018, *ApJ*, 861, 107, doi: [10.3847/1538-4357/aac9b8](https://doi.org/10.3847/1538-4357/aac9b8)
- Lin, Z., Calzetti, D., Kong, X., et al. 2020, *ApJ*, 896, 16, doi: [10.3847/1538-4357/ab9106](https://doi.org/10.3847/1538-4357/ab9106)
- Longmore, S. N., Kruijssen, J. M. D., Bastian, N., et al. 2014, in *Protostars and Planets VI*, ed. H. Beuther, R. S. Klessen, C. P. Dullemond, & T. Henning, 291, doi: [10.2458/azu\\_uapress.9780816531240-ch013](https://doi.org/10.2458/azu_uapress.9780816531240-ch013)
- Ma, J., Zhou, X., & Chen, J. 2004a, *A&A*, 413, 563, doi: [10.1051/0004-6361:20031556](https://doi.org/10.1051/0004-6361:20031556)
- Ma, J., Zhou, X., Chen, J., et al. 2002a, *AJ*, 123, 3141, doi: [10.1086/340361](https://doi.org/10.1086/340361)
- . 2002b, *AcA*, 52, 453, <https://arxiv.org/abs/astro-ph/0211317>
- Ma, J., Zhou, X., & Chen, J.-S. 2004b, *ChJA&A*, 4, 125, doi: [10.1088/1009-9271/4/2/125](https://doi.org/10.1088/1009-9271/4/2/125)
- Ma, J., Zhou, X., Chen, J.-S., et al. 2002c, *ChJA&A*, 2, 197, doi: [10.1088/1009-9271/2/3/197](https://doi.org/10.1088/1009-9271/2/3/197)
- Ma, J., Zhou, X., Kong, X., et al. 2001, *AJ*, 122, 1796, doi: [10.1086/323098](https://doi.org/10.1086/323098)
- Martin, D. C., Fanson, J., Schiminovich, D., et al. 2005, *ApJL*, 619, L1, doi: [10.1086/426387](https://doi.org/10.1086/426387)
- Massey, P., McNeill, R. T., Olsen, K. A. G., et al. 2007, *AJ*, 134, 2474, doi: [10.1086/523658](https://doi.org/10.1086/523658)
- Massey, P., Olsen, K. A. G., Hodge, P. W., et al. 2006, *AJ*, 131, 2478, doi: [10.1086/503256](https://doi.org/10.1086/503256)
- Messa, M., Adamo, A., Calzetti, D., et al. 2018, *MNRAS*, 477, 1683, doi: [10.1093/mnras/sty577](https://doi.org/10.1093/mnras/sty577)
- Meurer, G. R., Heckman, T. M., & Calzetti, D. 1999, *ApJ*, 521, 64, doi: [10.1086/307523](https://doi.org/10.1086/307523)
- Muñoz-Mateos, J. C., Gil de Paz, A., Boissier, S., et al. 2007, *ApJ*, 658, 1006, doi: [10.1086/511812](https://doi.org/10.1086/511812)
- Relaño, M., & Kennicutt, Robert C., J. 2009, *ApJ*, 699, 1125, doi: [10.1088/0004-637X/699/2/1125](https://doi.org/10.1088/0004-637X/699/2/1125)
- Rieke, G. H., Young, E. T., Engelbracht, C. W., et al. 2004, *ApJS*, 154, 25, doi: [10.1086/422717](https://doi.org/10.1086/422717)
- Ryon, J. E., Gallagher, J. S., Smith, L. J., et al. 2017, *ApJ*, 841, 92, doi: [10.3847/1538-4357/aa719e](https://doi.org/10.3847/1538-4357/aa719e)
- Sarajedini, A., & Mancone, C. L. 2007, *AJ*, 134, 447, doi: [10.1086/518835](https://doi.org/10.1086/518835)
- Schlafly, E. F., & Finkbeiner, D. P. 2011, *ApJ*, 737, 103, doi: [10.1088/0004-637X/737/2/103](https://doi.org/10.1088/0004-637X/737/2/103)
- Shabani, F., Grebel, E. K., Pasquali, A., et al. 2018, *MNRAS*, 478, 3590, doi: [10.1093/mnras/sty1277](https://doi.org/10.1093/mnras/sty1277)
- Sharma, S., Corbelli, E., Giovanardi, C., Hunt, L. K., & Palla, F. 2011, *A&A*, 534, A96, doi: [10.1051/0004-6361/201117812](https://doi.org/10.1051/0004-6361/201117812)
- Silva-Villa, E., Adamo, A., Bastian, N., Fouesneau, M., & Zackrisson, E. 2014, *MNRAS*, 440, L116, doi: [10.1093/mnrasl/slu028](https://doi.org/10.1093/mnrasl/slu028)
- Smith, L. J., Crowther, P. A., Calzetti, D., & Sidoli, F. 2016, *ApJ*, 823, 38, doi: [10.3847/0004-637X/823/1/38](https://doi.org/10.3847/0004-637X/823/1/38)
- Stanway, E. R., Chrimes, A. A., Eldridge, J. J., & Stevance, H. F. 2020, *MNRAS*, 495, 4605, doi: [10.1093/mnras/staa1166](https://doi.org/10.1093/mnras/staa1166)
- Stanway, E. R., & Eldridge, J. J. 2018, *MNRAS*, 479, 75, doi: [10.1093/mnras/sty1353](https://doi.org/10.1093/mnras/sty1353)
- Toribio San Cipriano, L., García-Rojas, J., Esteban, C., Bresolin, F., & Peimbert, M. 2016, *MNRAS*, 458, 1866, doi: [10.1093/mnras/stw397](https://doi.org/10.1093/mnras/stw397)
- U, V., Urbaneja, M. A., Kudritzki, R.-P., et al. 2009, *ApJ*, 704, 1120, doi: [10.1088/0004-637X/704/2/1120](https://doi.org/10.1088/0004-637X/704/2/1120)
- Vázquez, G. A., & Leitherer, C. 2005, *ApJ*, 621, 695, doi: [10.1086/427866](https://doi.org/10.1086/427866)
- Whitmore, B. C., Chandar, R., Bowers, A. S., et al. 2014, *AJ*, 147, 78, doi: [10.1088/0004-6256/147/4/78](https://doi.org/10.1088/0004-6256/147/4/78)
- Whitmore, B. C., Zhang, Q., Leitherer, C., et al. 1999, *AJ*, 118, 1551, doi: [10.1086/301041](https://doi.org/10.1086/301041)
- Whitmore, B. C., Chandar, R., Lee, J., et al. 2020, *ApJ*, 889, 154, doi: [10.3847/1538-4357/ab59e5](https://doi.org/10.3847/1538-4357/ab59e5)
- Wofford, A., Charlot, S., Bruzual, G., et al. 2016, *MNRAS*, 457, 4296, doi: [10.1093/mnras/stw150](https://doi.org/10.1093/mnras/stw150)
- Xiao, L., Stanway, E. R., & Eldridge, J. J. 2018, *MNRAS*, 477, 904, doi: [10.1093/mnras/sty646](https://doi.org/10.1093/mnras/sty646)
- Zackrisson, E., Rydberg, C.-E., Schaerer, D., Östlin, G., & Tuli, M. 2011, *ApJ*, 740, 13, doi: [10.1088/0004-637X/740/1/13](https://doi.org/10.1088/0004-637X/740/1/13)

Zombeck, M. V. 1990, Handbook of space astronomy and astrophysics, 100